

INTERDISCIPLINARY DOCTORAL SCHOOL

Faculty of Material Science and Engineering

Eng. **Ioana BORȘAN**

The influence of structural design on electrical, thermal, mechanical and tribological properties of TiN and (Ti,Al)N coatings prepared by reactive magnetron sputtering.

SUMMARY

Scientific supervisor

Prof. dr. eng. **Daniel MUNTEANU**

BRAȘOV, 2024

Summary

The protection of materials by coating them with thin films has proved to be one of the most versatile ways to improve their performance in the most diverse situations. Numerous relationships have been illustrated about the best combination of materials to use as a coating and its relationship to the properties that are intended to be achieved.

Currently, the number of materials on which the designation "hard" falls is already quite significant and it is therefore increasingly important to establish a criterion for selecting the best combination of materials to use. This task will not always be easy to accomplish, as the inherent specificity of each thin film/substrate system requires different types of compromises. The decision will be even more difficult if it is possible to choose the material to be used in the form of thin film or in solid form. However, solid materials are widely known for their low ductility, as one of their basic characteristics and therefore are quite brittle. As a consequence, their use in applications with predominant intense loads and wear is restricted. In these cases, the alternative is usually to use a more ductile material, coated with a thin, hard, wear-resistant thin film, or to develop a new solid material with the same properties mentioned above.

Although research is currently divided between these two guidelines, the physics of thin films will have a greater field of development, due to the characteristics they support. Currently, the number of well-studied coating for the most diverse application reaches high values. Above all, the need to study the various interactions between the thin film and substrate emerges from this.

For this research, the binary compound, TiN and the ternary compound, (Ti,Al)N coatings have been chosen, since these are the most popular coatings, for enhancing various properties.

The coatings listed above have wear resistance, inertia, are capable to reduce friction and are usually used on cutting tools, punches, dies and injection mold components to improve tool life two to ten times, or more, over uncoated tools.

Everything started by questioning what will happen if only the nanostructure of the thin films would be modified and the composition would be kept the same. After the research was done, the results turned out to be quite unexpected, but extremely useful. For example: coatings like TiN can be either be conductive or insulating, just by varying the nanostructured design.

In this sense, the present thesis is structured in 5 chapters, which contain the information about the changes that appear when the nanostructured coating designs are changed, even if the same composition is kept.

The first chapter, **Surface engineering - an overview; the general objectives of the doctoral thesis**, is giving the reader on overview about the surface engineering, the importance of different treatments applied on the surface of the parts and objects used on the daily basis. The main objectives of the thesis are presented, together with the overview on this subject.

In the second chapter, **Deposition of coatings and thin films using plasma-assisted techniques**, the deposition processes of thin films, using plasma-assisted techniques are described.

It is impossible to discuss about plasma-assisted techniques without explaining the importance of vacuum.

In this context, the second chapter includes also aspects of vacuum and electrical discharges in gases and information about the plasma state. After presenting the vacuum aspects, magnetron-sputtering technique will be detailed. In the conclusion of the second chapter, general aspects of TiN and (Ti,Al)N coatings will be presented.

The third chapter, **Deposition and characterization of TiN and (Ti,Al)N coatings with a normal columnar structure growth**, explains the deposition processes used in obtaining TiN and

(Ti,Al)N coatings for this research. After presenting the deposition technique used, the chemical-, structural-, morphological-, thermal-, optical-, electrical-, mechanical- and tribological properties are presented, together with the corrosion behaviour of TiN and (Ti,Al)N coatings deposited with normal columnar structure growth, but with different N₂ and Al content.

The fourth chapter, **Deposition and characterization of TiN and (Ti,Al)N coatings with inclined and zigzag structural designs**, information about GLAD technique used to obtain different nanostructured designs, are given. In the fourth chapter, the following characterizations for different nanostructured designed TiN and (Ti,Al)N deposited coatings, are shown: chemical-, structural-, morphological-, thermal-, optical-, electrical-, mechanical-, tribological properties and corrosion behaviour.

Chapter five, **Final conclusions**, gives the final overview of the most important conclusions from each chapter.

Changing the structural design, whether it is for an inclined or zigzag form, it has a significant impact on the thermal and electrical characteristics. According to these aspects, two main objectives can be outlined for this work:

O1. To study the influence of **the composition** of TiN and (Ti,Al)N thin-films (grown normally on the surface of the substrate) on their general properties;

O2. To study the influence of **the structural design** of TiN and (Ti,Al)N thin-films on their general properties (for the most convenient compositions - previously determined).

Related to these objectives, all the deposited coatings are characterized by structure and morphology. At the same time, chemical-, thermal-, optical-, electrical-, mechanical- and tribological properties together with the corrosion behaviour of TiN and (Ti,Al)N coatings are to be studied.

In order to obtain the coatings to fulfil the first objective, magnetron-sputtering technique was used. By PVD magnetron sputtering, two sets of samples were prepared: first one with TiN coatings, where the structure is columnar (normal on the substrate surface - inclination angle - 0°) but the N_2 flow increases from 0 to 4 sccm and the second one where (Ti,Al)N coatings were deposited, by varying the Al content, placing different numbers of Al pallets on the Ti target. Firstly the deposition started with 150 pallets, with a weight of $\sim 1\text{g/pallet}$ glued with Ag paste on the erosion zone of Ti target. After, the number of pallets was decreased to 100, then to 50 and finally to a number of 25p.

In this research, a vacuum chamber together with one magnetron, one DC power supply and a conventional substrate holder were used (figure 1).

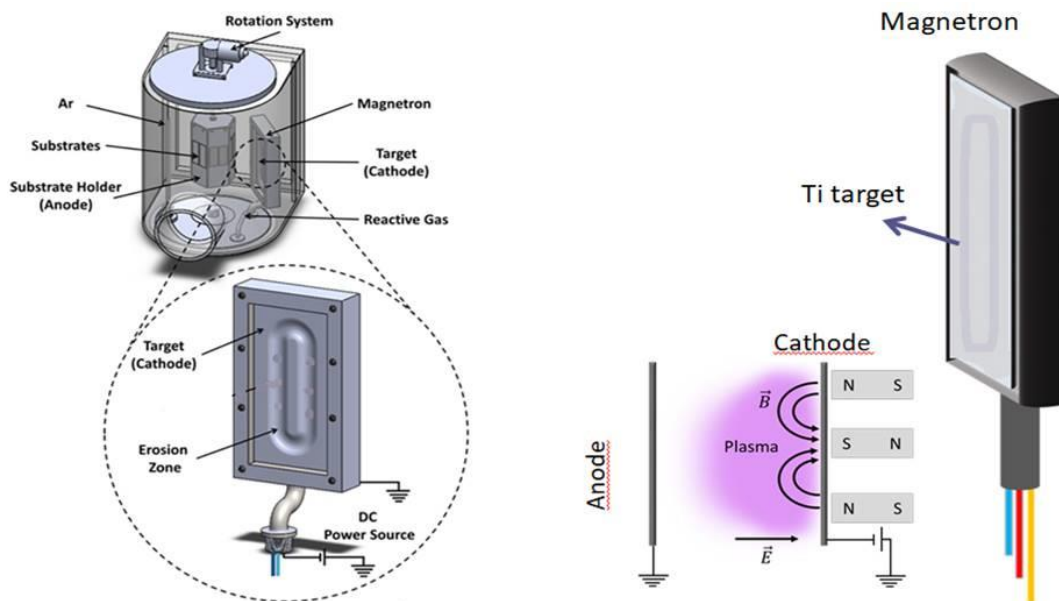


Figure 1 Deposition equipment.

At a current density of 75 A/m^2 , the target was sputter-deposited in a gas environment of Ar (flow of 25 sccm - partial pressure of $3.5 \times 10^{-1} \text{ Pa}$) and N_2 . For every deposition, the base pressure was maintained below $5 \times 10^{-4} \text{ Pa}$. To achieve a consistent thickness of around $2.0 \pm 0.2 \text{ }\mu\text{m}$ for all the samples, the deposition duration was modified. Glass, steel and silicon (p-type, monocrystalline, boron-doped, [100] oriented) were the

substrates utilized for all depositions. They were positioned in a grounded hexagonal substrate holder 70 mm away from a pure titanium rectangle target (200 x 100 x 6 mm³, 99.99% purity). Due to variations of N₂ flow and Al content, the deposition rate and target potential present some variations.

Chemical and structural properties of TiN and (Ti,Al)N coatings with variation of composition

As shown in figure 2 (a), the evolution of the chemical composition of the samples made with TiN validates the change of growth modes (corresponding to sub- to over-stoichiometric condition). The sample created at a 3 sccm nitrogen flow rate has a near stoichiometric composition (52 at.% Ti and 48 at.% N₂; N/Ti ratio: 0.92), which is in line with the target potential's maximum value.

In contrast, the nitrogen content of the samples rises with N₂ gas fluxes up to 3 sccm in the metallic regime (figure 2 (a)). The result can be attributed to the continuous insertion of N₂ atoms into the Ti crystalline lattice, although at typical operating circumstances, the flow is too little to seriously contaminate the target.

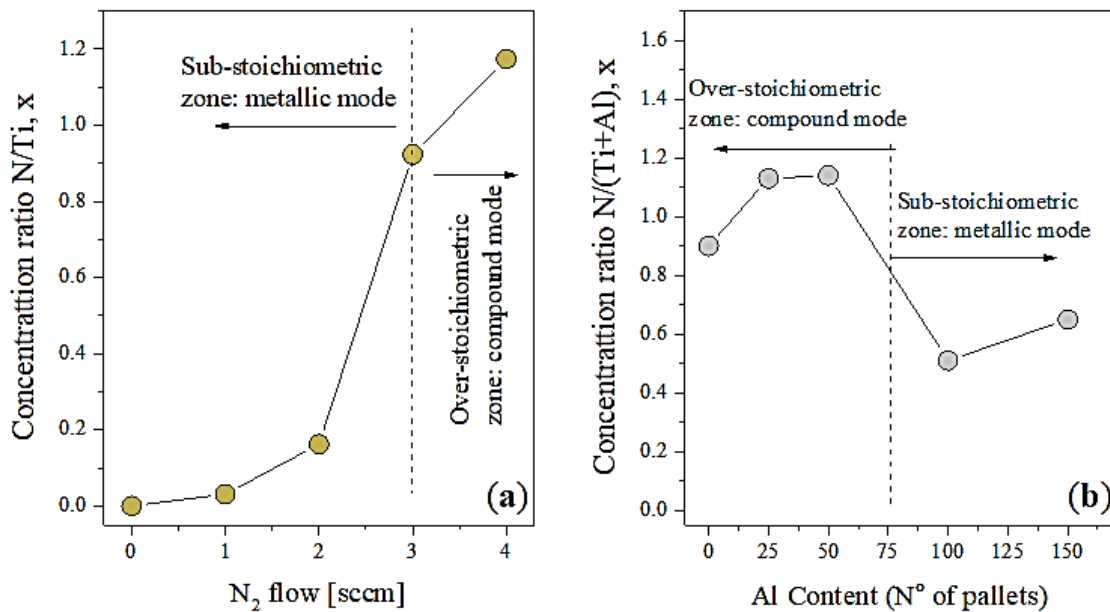


Figure 2 (a) Evolution of Ti and N₂ concentration ratio
(b) Evolution of Ti, Al and N₂ concentration ratio.

By the same reasoning, the deposition rate of the sub-stoichiometric samples is not significantly different as the sputtering yield of Ti atoms from the target surpasses the poisoning effects.

The composition, structure and characteristics of a (Ti,Al)N coating undergo significant changes when the amount of aluminum (Al) in the coating rises. The main cause of these modifications is the substitution of Al atoms for Ti atoms in the crystal lattice, which has an impact on the microstructure and performance properties of the material.

The concentration of Al in the TiN structure it is presented in figure 2 (b). There is a direct correlation between the target potential, deposition rate for different Al content.

As Al is material which has a higher sputtering rate, the deposition rate increases. As the results show, the (Ti,Al)N coatings are either under or over-stoichiometric and therefore, the mechanical and tribological properties will be lower in comparasion with the stroichiometric version of thin films.

The majority of materials' surface response, especially those of thin films, is greatly influenced by the unique crystalline structure of those materials and any potential changes to that structure over time. In this regard, it is crucial to characterize the crystalline structure of every given thin film system in order to better understand its unique behaviour, particularly when in use.

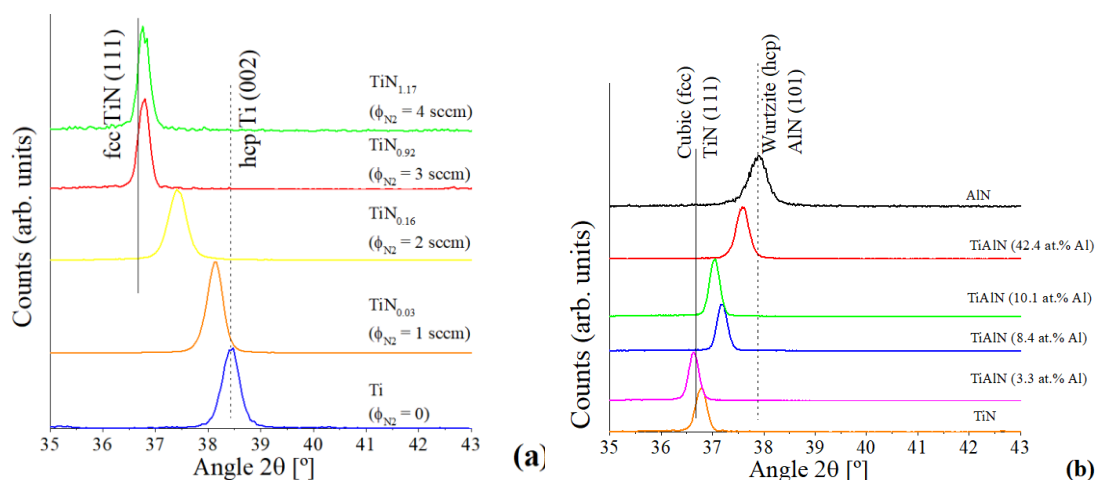


Figure 3 Evolution of the XRD patterns of (a) TiN_x films; (b) $TiAl_xN$ coating.

Figure 3 depicts the development of TiN_x samples and Ti-Alx-N coatings that were created for this thesis' XRD diffraction patterns.

For the set of samples prepared in standard geometry (series 1), the XRD diffraction patterns, figure 3 (a), demonstrate the formation of a hexagonal-Ti phase (space group P63/mmc) with a high (002) orientation for the Ti reference sample (flow = 0).

A characteristic FCC Ti-N structure (space group Fm-3m) is resulting from the progressive movement of the diffraction peaks to lower diffraction angles as the N_2 content increases.

This structure is particularly evident for the close- and over-stoichiometric samples, $TiN_{0.92}$, respectively $TiN_{1.17}$.

This process corresponds with the chemical composition of the films and the expectations of the Ti-N phase diagram, which is basically understood to be a titanium crystal that is "interstitial" where nitrogen fills in the structural gaps, despite its high complexity.

The data indicates that this is the case for the samples $TiN_{0.03}$ and $TiN_{0.16}$, which were prepared with N_2 fluxes of 1 and 2 sccm, respectively and may likewise be included in a type of transition zone towards the production of the characteristic TiN face-centered cubic structure.

The comparison between the diffraction patterns of HCP Ti and FCC TiN and these two samples is shown in figure 3(a).

When Al is added into the TiN matrix, everything changes. As the aluminum content in (Ti,Al)N increases, the diffraction peaks may shift due to changes in the lattice parameter (figure 3 (b)).

Aluminum atoms are smaller than titanium atoms, causing a slight lattice contraction and shifting peaks to higher angles. The (Ti,Al)N thin films samples present a cubic (FCC) structure presented in figure 3 (b), which shows a strong (111) texture followed by small (311) peaks (figure 3(b)).

Morphological properties of TiN and (Ti,Al)N coatings with variation of composition

As can be noticed in figure 4 (a-d) the films made for the TiN_x series with normal (structural) configuration exhibit microstructures within the transition from Zones T and II of the Structural Zone Model (SZM), which is consistent with J.A. Thornton, I. Petrov et al. growth zone models. Those findings have been also vetted by B.A. Movchan et al. and extended by Mahieu et al. When more N_2 is incorporated into the Ti structure, Zone II (planes of lowest surface energy and greatest thermodynamic stability) evolves into Zone T (lowest growing rate planes facing the geometrically quickest growth direction) (high N_2 flow rates).

Figure 4 (a) and (b) show columnar structures with roughly straight columns in films made with N/Ti ratios of 1 (N_2 flow rate of 3 sccm) and the high deposition rate values take advantage of quick surface diffusion and the appearance of recrystallization phenomena to increase the columns' lateral size. Zone T, figures 4 (c) and (d), demonstrate the development of V-shaped faceted columns with some noticeable tendency towards densification and shrinking of the columns, which is constant with the reduced deposition rate values. These films are close and over-stoichiometric (N_2 flow rates 3 sccm).

The depositions conducted out with Ti-Al_x-N have at the beginning a columnar structure. As the Al content increases, the growth mode shifts from a columnar to a more continuous and uniform layer, which is a direct response of reduced surface roughness because of the small grain size of Al particles. At lower Al content, the coating may exhibit a columnar structure with limited crystallinity within the Zone 1 and transition Zone, described by Thornton Model. As the Al concentration increases the coating transitions to a high degree of crystallinity, also known as Zone 3. Zone 3 represents a high crystallinity due to high adatom mobility.

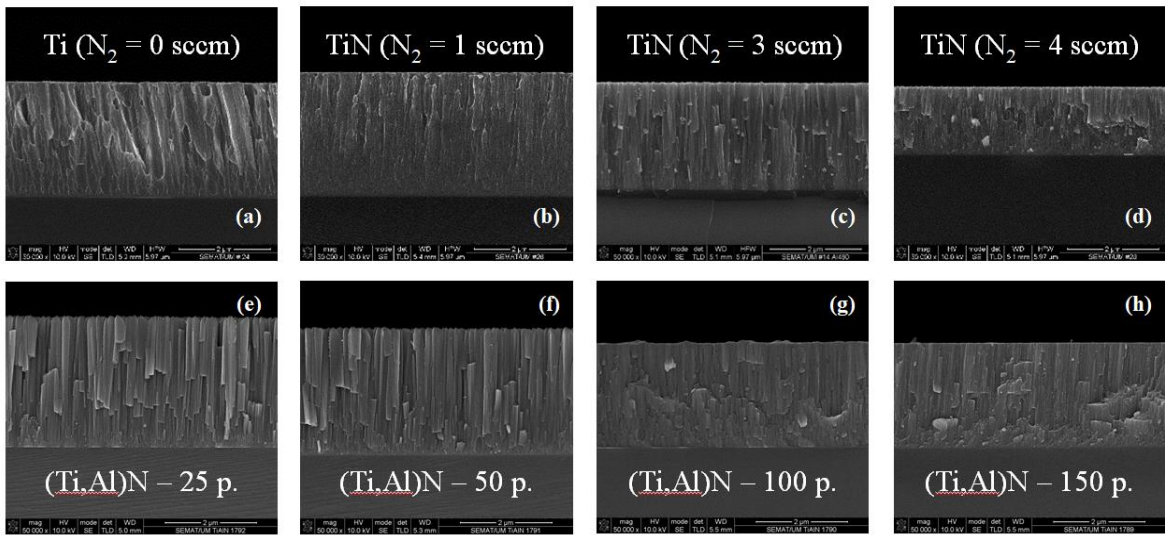


Figure 4 Cross-section SEM images of the two set of samples: (a-d) TiN_x series (e-h) $(Ti,Al)N$ series.

The variations brought about by increasing the incidence flux of the sputtered atoms are depicted in figure 5 as varied values of RMS surface roughness. The findings demonstrate that $(Ti,Al)N$ films are smoother and than TiN coatings,. As Al content decreases, the thin films become progressively rougher.

$(Ti,Al)N$ coatings are smoother than TiN coatings primarily due to grain refinement, which results in smaller, more densely packed grains and a nanocrystalline structure that reduces surface roughness.

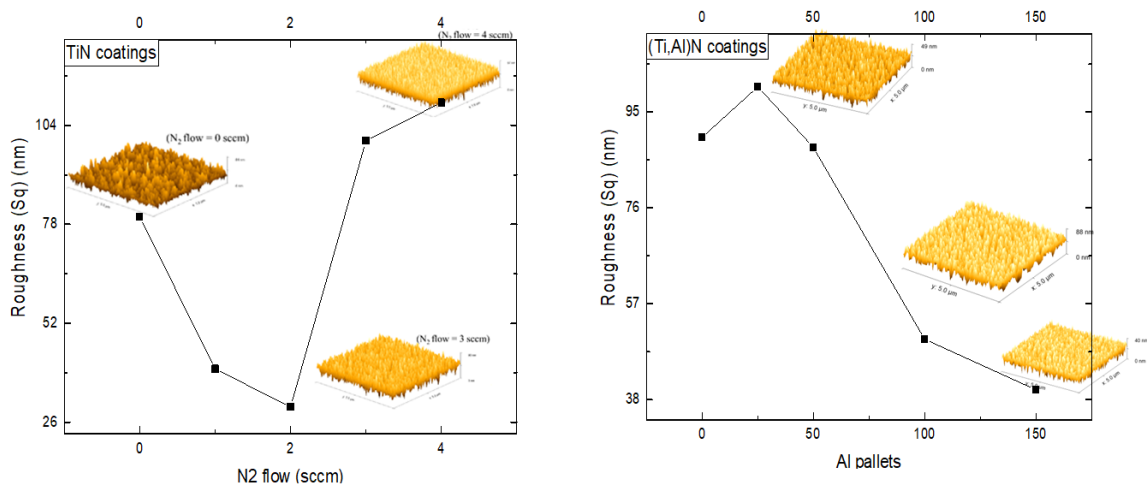


Figure 5 Evolution of the surface roughness values of the two series of samples; (a) TiN by varying the N_2 concentration; (b) $(Ti,Al)N$ by changing the Al content.

The addition of aluminum enhances adatom mobility and stabilizes the cubic phase, promoting uniform film growth and reducing defects such as porosity and voids.

Additionally, the formation of a smooth aluminum oxide layer on (Ti,Al)N coatings further contributes to their smoother surface.

The set of findings shown in figures 2 through 5 demonstrate once more that, even though all the samples were made with nearly identical deposition parameters (thickness, target current) there are numerous differences throughout the results. It is well known that in order to customize the surface characteristics of a specific thin film system, changing the composition of the coating is needed. For the majority of technical and industrial applications, including the biomedical sector for cellular growth enhancement/adhesion, chemical and physical sensing, mechanical and tribological applications, among many others, the tailoring of the surface roughness and the sort of columnar growth is of most importance.

Thermal properties of TiN and (Ti,Al)N coatings with variation of composition

Figures 6 and 7 display the results of direct measurements made on the various collections of samples. Both the effusivity ratio and the thermal effusivity values for the series 1 constructed in conventional geometry exhibit similar behaviour, rising for the sample with 1 sccm and then dropping as the flow rate increases. In general, it is predicted that the thermal characteristics would drop as the N/Ti ratio rises because additional nitrogen results in less dense and more porous samples, which reduces the efficiency of heat diffusion. Throughout the case, it is clear that the thermal diffusivity and thermal effusivity both changes as the concentration of N₂ and Al.

Even if not computed explicitly, it is obvious to draw the conclusion that the films' thermal conductivity likewise declines in line with the general trend.

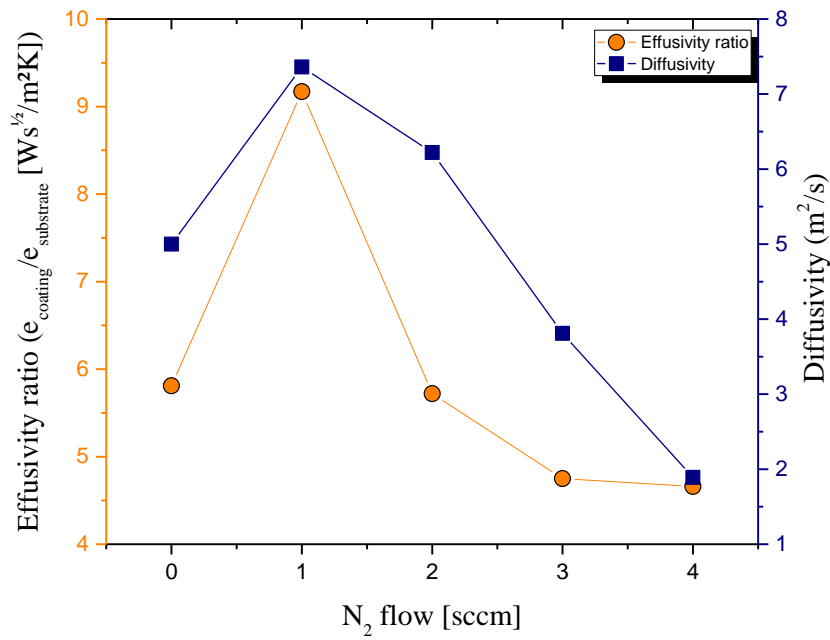


Figure 6 Evolution of the effusivity ratios and the diffusivity values for TiN_x series with variation of N_2 concentration.

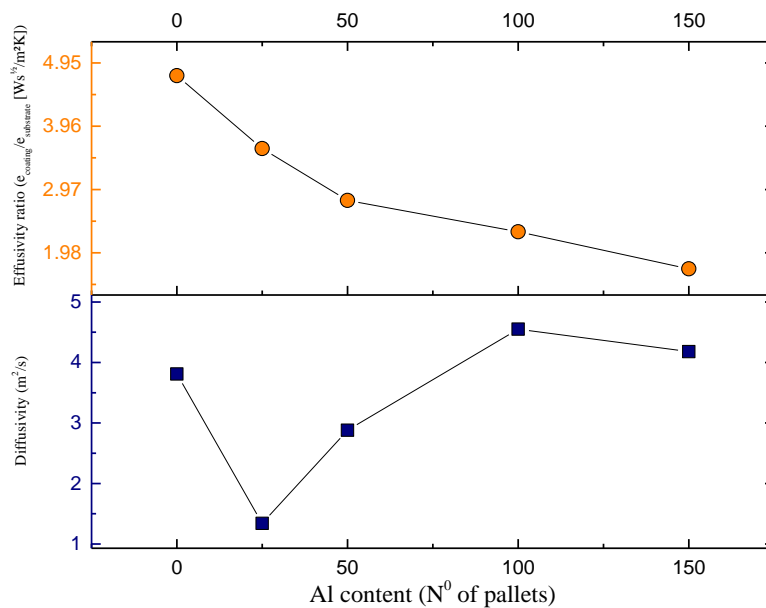


Figure 7 Evolution of the effusivity ratios and the diffusivity values for $(Ti,Al)N$ by changing the Al content.

Optical properties of TiN and (Ti,Al)N coatings with variation of composition

Further, the evolution of the films' colour coordinates, shown in figures 8 and 9, follows the changes in reflectivity and exhibits a similar evolution pattern.

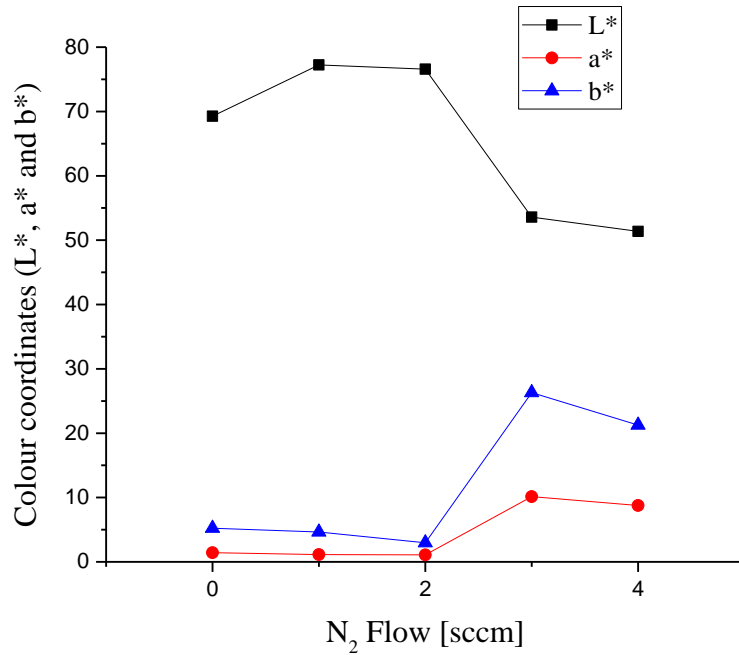


Figure 8 Evolution of the colour coordinates of TiN by varying the N₂ concentration.

This graphic shown in figure 8 demonstrates the results' infamous consistency by showing the same two separate zones for the samples generated by normal incidence (series 1). The sub-stoichiometric samples from series 1 (N/Ti ratio 1), which include the Ti reference sample, show the greatest values of this coordinate, which is a hallmark of the metallic-like samples, in terms of brightness values, L*.

One must bear in mind that interactions between incoming photons and free electrons affect the brightness of metallic materials in order to comprehend the variations between the samples of the sub- and over-stoichiometric zones from series 1. Hence, a drop in the density of states at the Fermi surface should be related to a decrease in the brightness for samples generated with high nitrogen concentrations (N₂ flow = 3 sccm). The yellowing of the surface colour tones is consistent with the significant rise in both values seen in a* and b* colour coordinates.

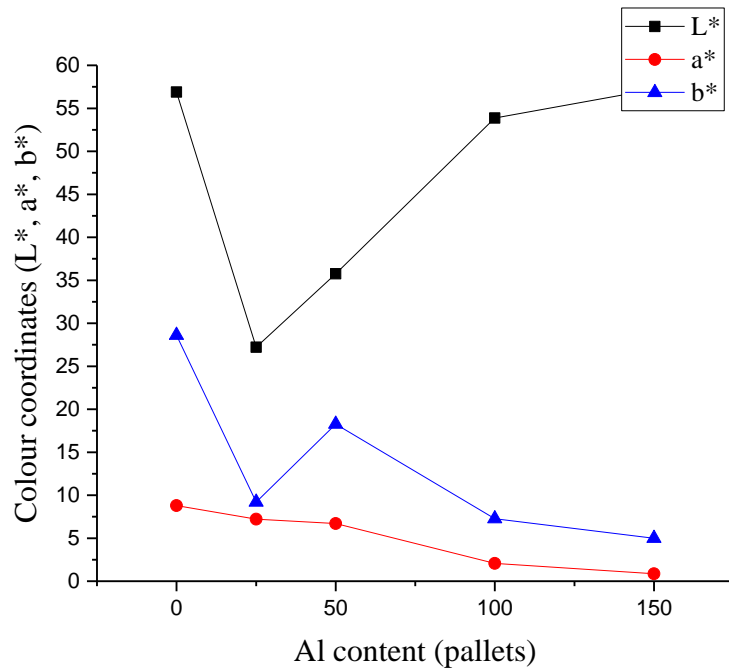


Figure 9 Evolution of the colour coordinates of (Ti,Al)N by changing the Al content.

It is feasible to see a considerable shift in the optical behaviour between the two sets of samples, as the Al content rises (figure 9). The samples' colour changes from light gray to dark gray as the number of increases. Together with the samples' darkening, the yellow and blue coordinate (b^*) falls dramatically as well. The small decrease in the red and green coordinate (a^*) indicates a propensity for reddish tones.

The evolution of colour coordinates as a function of the deposition parameters, seen in figure 10, represented by the so-called colour difference parameter, ΔE^* , is another important subject. Even if, visually, the coatings from each set of sample might seem not so different from one another, considerable deviations can be spotted (figure 10). To assess a sample's surface quality and suitability for a particular application, it is essential to compare it to a reference sample that has a similar colour to the sample in question. For the first series, the reference sample is pure Ti (figure 10 (a)) and for the second series, the (Ti,Al)N coatings, the TiN close to stoichiometric it is used (figure 10 (b)).

The roughness, morphology and colour coordinates of TiN and (Ti,Al)N coatings are interconnected and collectively influence the overall appearance and optical properties of the coatings. TiN coatings have a more columnar grain structure, leading to higher surface roughness.

This roughness scatters more light, affecting reflectivity and appearance.

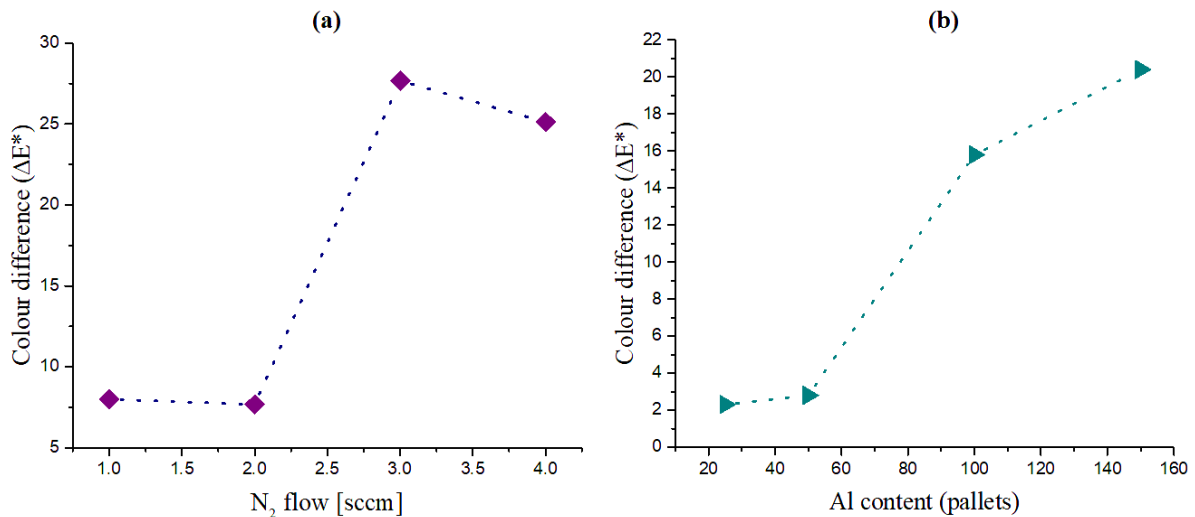


Figure 10 Evolution of the colour difference for the thin films:
(a) TiN by varying the N_2 concentration;
(b) (Ti,Al)N by changing the Al content.

On the other hand, (Ti,Al)N thin films tend to have a finer, nanocrystalline structure, as the Al content increases, resulting in a smoother surface.

This reduced roughness minimizes light scattering and contributes to a more uniform appearance. Given that TiN and (Ti,Al)N have distinct colour coordinates due to their different compositions and morphologies, ΔE^* provides a clear analysis of this difference.

A higher ΔE^* value indicates a more noticeable colour difference, reflecting the distinct optical properties and appearances of the two coatings (figure 10).

Electrical properties of TiN and (Ti,Al)N coatings with variation of composition

Figure 11 depicts the development of the thin films' resistivity for both series. The first inference to be made from this figure is that the evolution of electrical resistivity exhibits behaviour that is similar to that of the evolution of optical properties, namely, a notable difference can be seen between TiN serie (figure 11 (a)) and (Ti,Al)N set of samples (figure 11 (b)).

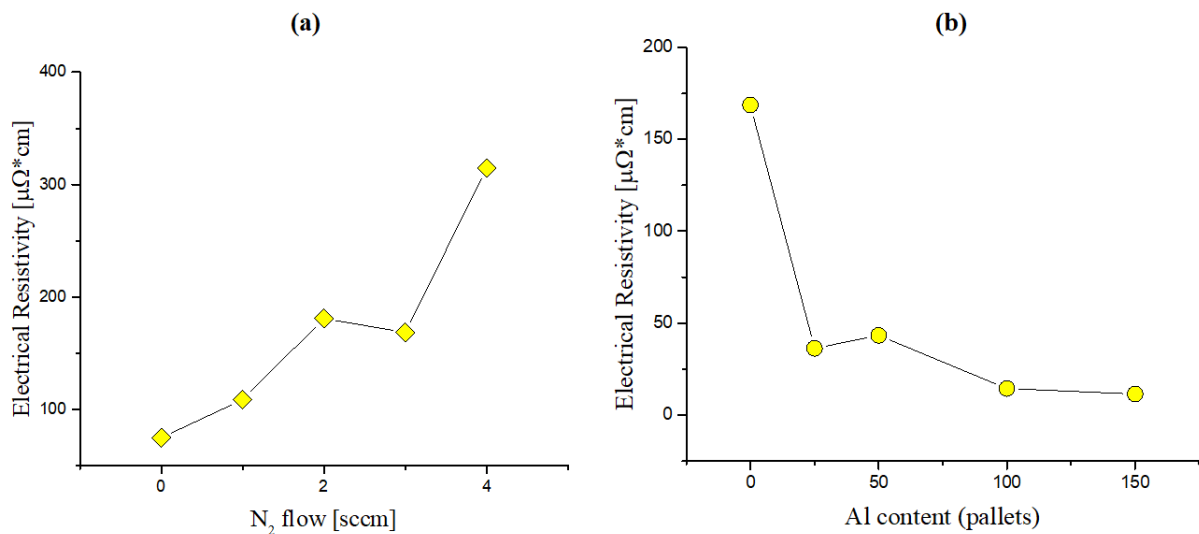


Figure 11 Evolution of the electrical resistivity of the thin films: **(a)** TiN by varying the N_2 concentration; **(b)** (Ti,Al)N by changing the Al content.

The films created with TiN, display a higher electrical resistivity in comparasion to (Ti,Al)N coatings. The values of the first set of samples increased one order of magnitude, highlighting once more the predominance of morphological features over composition and structural changes. The development of near and over-stoichiometric TiN compounds (N_2 flow rates higher than 3 sccm), well-known for the ceramic and less conductive properties, is caused by the addition of nitrogen to the titanium matrix.

Despite the increase in crystallite sizes in this zone, the influence of the scattering effects by the surface roughness

features, seems to be the major parameter to take into consideration for this fluctuation. The electrical resistivity of (Ti,Al)N coatings decreases with increasing Al content due to several key factors. Higher Al content stabilizes the cubic phase, improves crystalline quality and refines the grain structure, reducing grain boundaries and defects that impede electron flow.

Additionally, aluminum modifies the electronic band structure, enhancing electron mobility and contributes to a more homogeneous and dense microstructure. These combined effects facilitate better electron conductivity, resulting in lower resistivity. As it is presented in figure 11 (b), just a small amount of Al, declines drastically the electrical resistivity of (Ti,Al)N coatings.

Mechanical and tribological properties of TiN and (Ti,Al)N coatings with variation of composition

Figure 12 displays the mean loading-unloading curve of each deposition of both series from nanoindentation, process through which hardness and elastic modulus were measured. Even though the graphs from figure 12 don't seem to be very different from one another, actually, the differences are significant (figure 12).

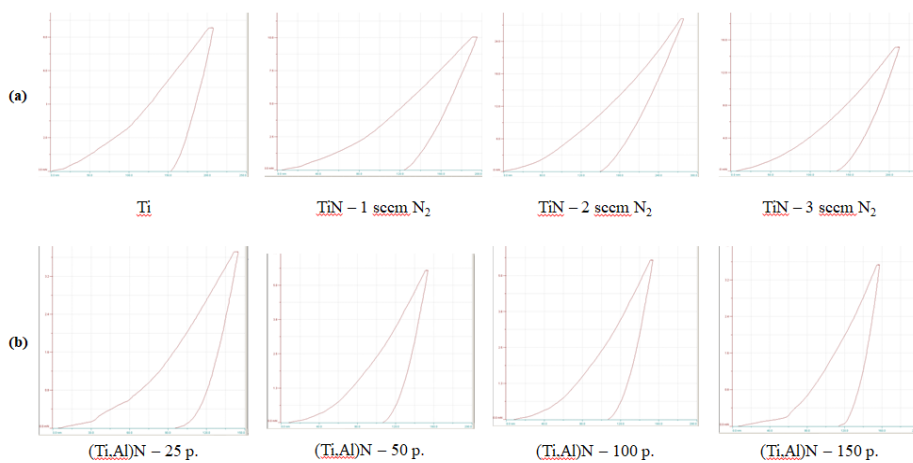


Figure 12 Indentation loading-unloading curves of: **(a)** TiN_x series with different N_2 flow; **(b)** (Ti,Al)N series with variation of Al content.

The hardness and elastic modulus of TiN coatings are highly dependent on the nitrogen content. In figure 13 it can be observed that, up to a N₂ flow of 3 sccm, hardness and elastic modulus are increasing and after this peak which represents the sample with 3 sccm of N₂ flow, the properties start to decrease. The strong covalent bonding between Ti and N₂ atoms in stoichiometric TiN coatings, significantly enhances hardness and elastic modulus.

Higher nitrogen leads to grain refinement and a denser microstructure, reducing defects and porosity. The improved bonding strength Ti and N₂ atoms enhance mechanical properties.

Additionally, the increased nitrogen content often results in beneficial compressive residual stress, further boosting hardness and elastic modulus.

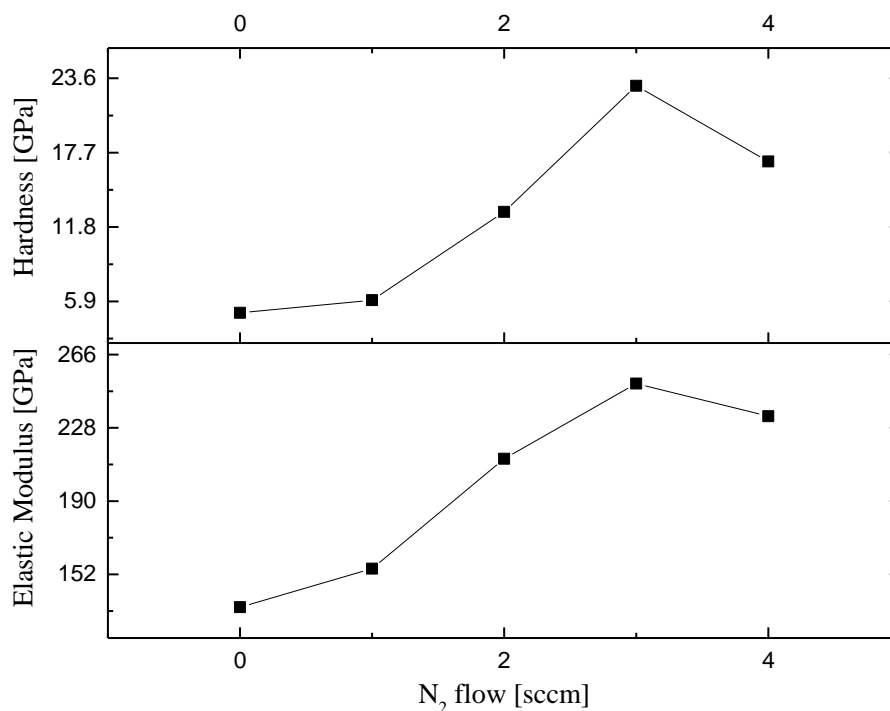


Figure 13 Evolution of hardness and elastic modulus for series 1 - TiN_x samples.

While optimal nitrogen content improves hardness and elastic modulus, excessive nitrogen can lead to the formation of suboptimal phases, increased defects, excessive residual stress and a less dense microstructure, ultimately compromising the coating's mechanical properties and performance.

Titanium aluminium nitride - (Ti,Al)N - coatings often exhibit higher hardness than TiN due to solid solution strengthening and grain refinement effects caused by aluminum addition. In order to have higher hardness in (Ti,Al)N coatings, it is crucial to make sure the thin films reached a stoichiometric composition, otherwise, if the deposited compound is under- or over-stoichiometric, the mechanical properties will decrease.

In the research case, as stoichiometry could not be reached and the coatings are either under- or over-stoichiometric (N_2 concentration is lower or higher than Al/Ti composition - figure 2 (b)), the mechanical properties are diminished (figure 14).

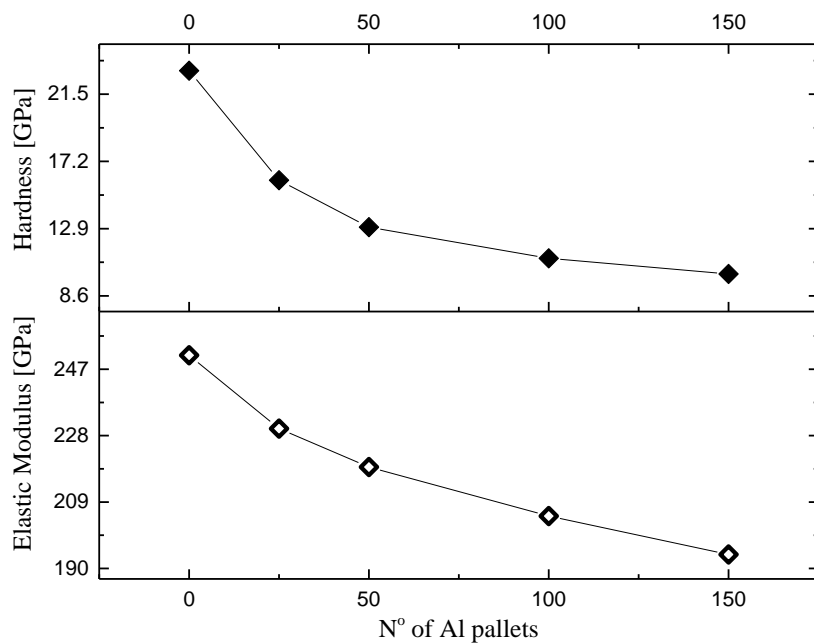


Figure 14 Evolution of hardness and elastic modulus for series 2 - (Ti,Al)N samples.

After the hardness and elastic modulus measurements, another important aspect is the capacity of the material to disperse energy at plastic deformation during loading, represented by the ratio - H^3/E^2 .

The H^3/E^2 ratio is a critical parameter for evaluating the toughness of coatings.

A higher H^3/E^2 ratio values indicate a good balance of hardness (resistance to indentation) and elasticity (stiffness), leading to enhanced durability and reduced cracking. Thus, this ratio is

useful for assessing the mechanical performance and overall toughness of hard coatings like TiN and (Ti,Al)N.

Figure 15 (a) shows that the close to stoichiometric coating - TiN_{0.92}, has the highest value, meaning that it displays the noblest property to resist plastic deformation.

As Al content increases, (Ti,Al)N coatings become more brittle, hence the thin films will have a diminished plastic deformation resistance (figure 15 (b)).

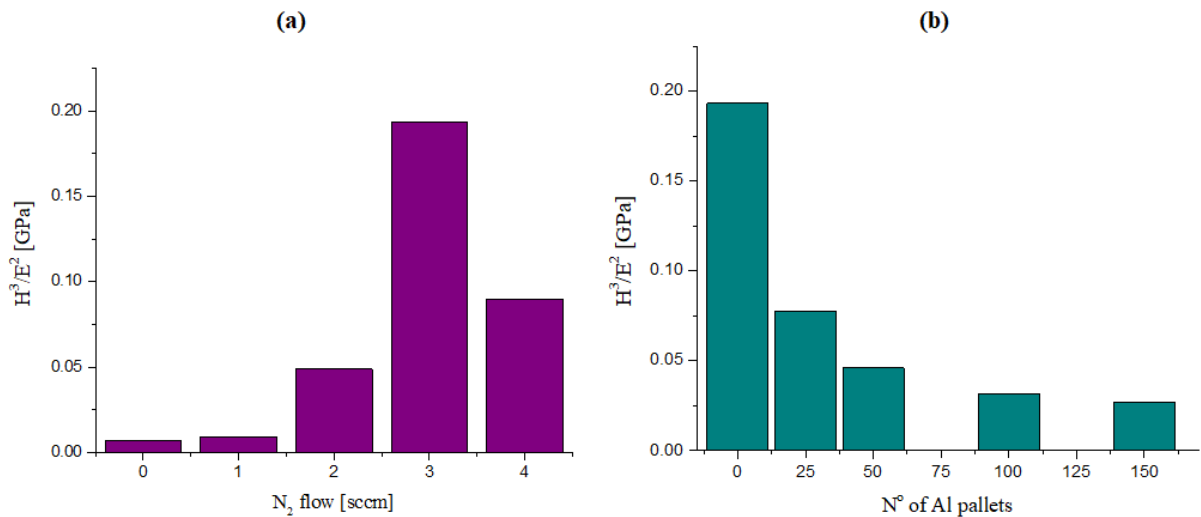


Figure 15 Evolution of H^3/E^2 ratio of:
(a) TiN_x series with different N₂ concentration;
(b) (Ti,Al)N coatings with different Al content.

The addition of N₂ to Ti coatings, forming titanium nitride (TiN) coatings, generally influences the critical load in several ways due to changes in mechanical properties, adhesion and microstructure.

TiN coatings are harder than pure Ti coatings, as it can be also observed in figure 13.

The higher hardness typically improves wear resistance and increases the critical load required to scratch or remove the coating. Enhanced hardness and wear resistance mean that the coating can withstand higher forces before failing, leading to a higher critical load (figure 16).

The introduction of N_2 improves the bonding strength between the coating and the substrate. Stronger bonds result in better adhesion, which increases the critical load (figure 16).

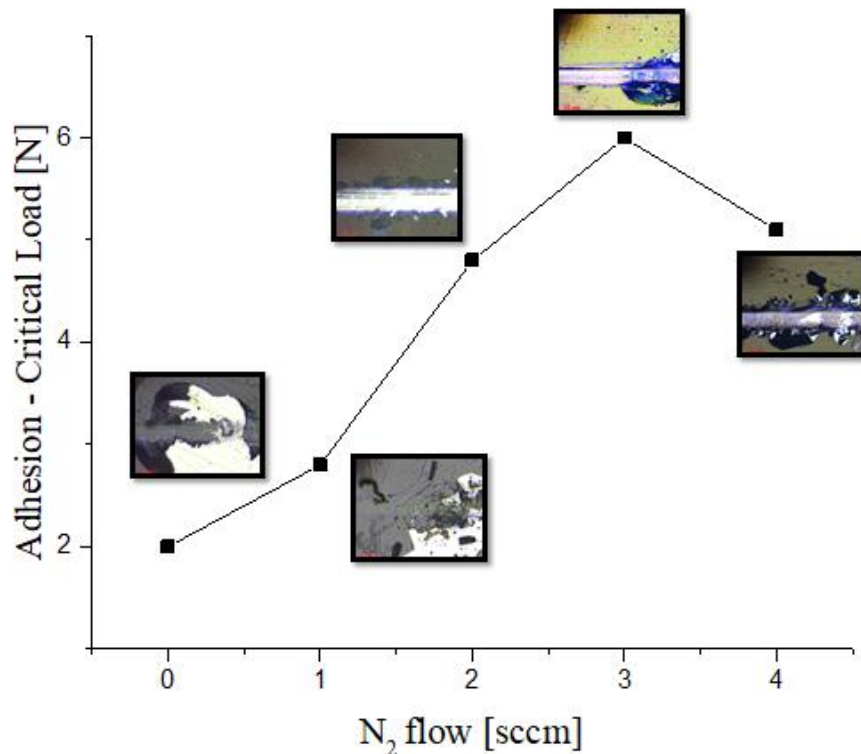


Figure 16 L_{C3} adherence critical load variation for series 1 - TiN coatings with variation of N_2 flow.

Achieving a stoichiometric balance (TiN_x where $x \approx 1$) is crucial because optimal N_2 content enhances adhesion properties, whereas too much or too little N_2 can result in weaker adhesion and lower critical loads, as it happens at the fourth sample, which contains too much N_2 .

Figure 17 displays the critical load of (Ti,Al)N coatings, which decrease even with moderate Al content due to microstructural changes that weaken grain boundaries and alter residual stress profiles.

Mixed phases, particularly the presence of hexagonal AlN and lattice distortion introduce weak points and reduce mechanical strength. Changes in the chemical and physical nature of the coating-substrate interface weaken adhesion mechanisms.

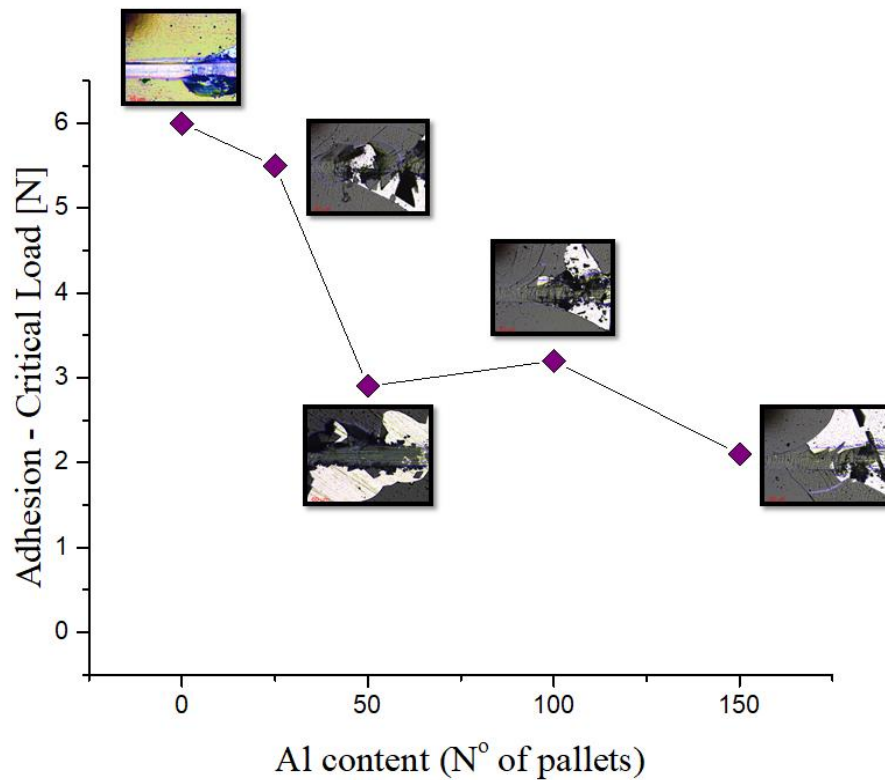


Figure 17 L_{C3} adherence critical load variation for series 2 - $(Ti,Al)N$ coatings with variation of Al content.

The tribometer was set to make 4 different paths having radii between 2 and 5 mm (figure 18).

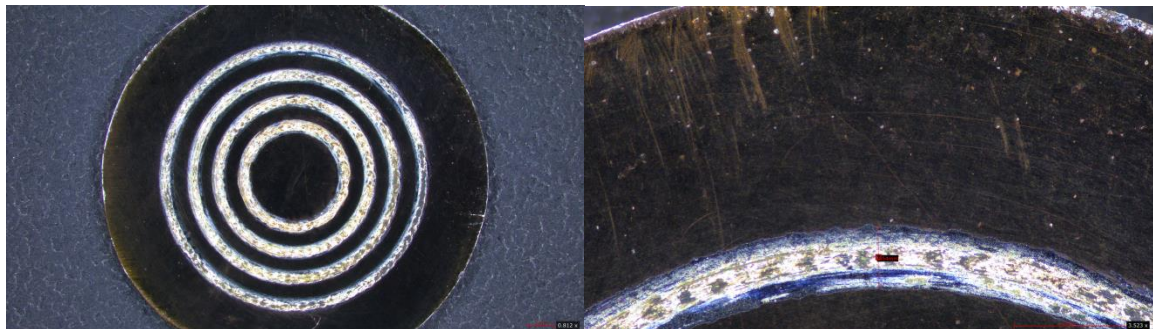


Figure 18 Wear paths of the $TiN_{0.92}$ coating with different radius from 2 to 5 mm.

Figure 19 shows the variation of the wear rate and friction coefficient of TiN_x series, which are directly linked to the roughness of the coatings (figure 5). Nitrogen incorporation affects the surface roughness of the coating, altering the contact area and frictional behaviour. Rougher surfaces lead to higher friction coefficients and accelerated wear due to increased asperity interactions.

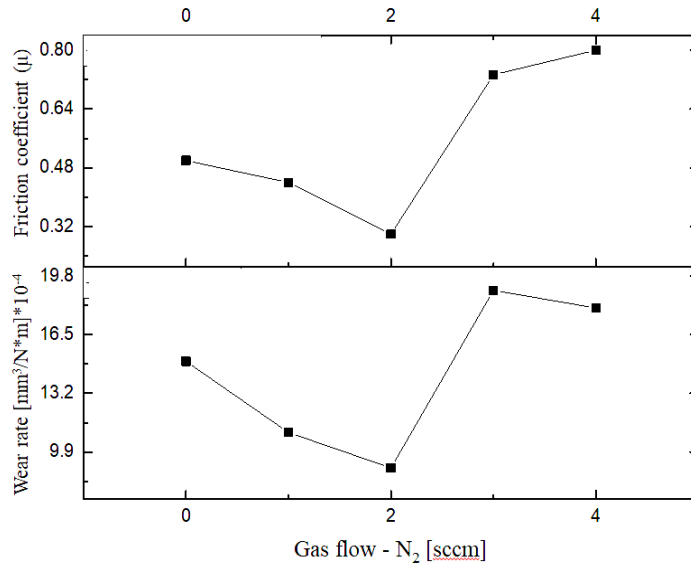


Figure 19 The variation of dynamic friction coefficient and wear rate for the first series - TiN_x samples.

As the microstructure is more refined due to the content of Al atoms, the roughness of the surface is smoother, resulting a decrease in wear rate and friction coefficient (figure 20).

Even though the tribological behaviour might be improved with (Ti,Al)N coatings in comparasion with TiN thin films, it is important to keep in mind that by adding Al into TiN matrix, the films tend to become more brittle due to their crystal structure and atomic bonding characteristics.

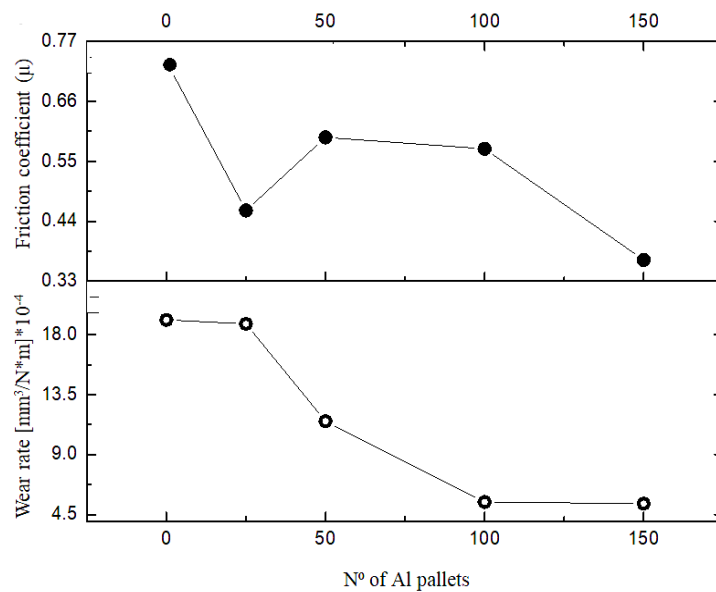


Figure 20 The variation of dynamic friction coefficient and wear rate for the second series - (Ti,Al)N samples.

However, due to their superior wear resistance and thermal stability, (Ti,Al)N coatings are preferred when friction is a challenge, because they can significantly extend the operational lifespan of cutting tools and wear components. This results in reduced downtime for tool change, increase productivity in manufacturing processes.

Results of TiN and (Ti,Al)N coatings with variation of structural design

Three different series of samples were prepared, the first two are TiN coatings and the third one (Ti,Al)N thin films.

The first set of samples was deposited by varying the flux angle of the sputtered particles ($\alpha = 40^\circ, 60^\circ$ and 80°) - measured in relation to the normal on the substrate surface and the second by designing two periods of zigzag thin films architected using the angles of the first set (figure 21).

A conventional TiN nitride thin film growing in an incidence normal to the substrate was also prepared for comparative purposes.

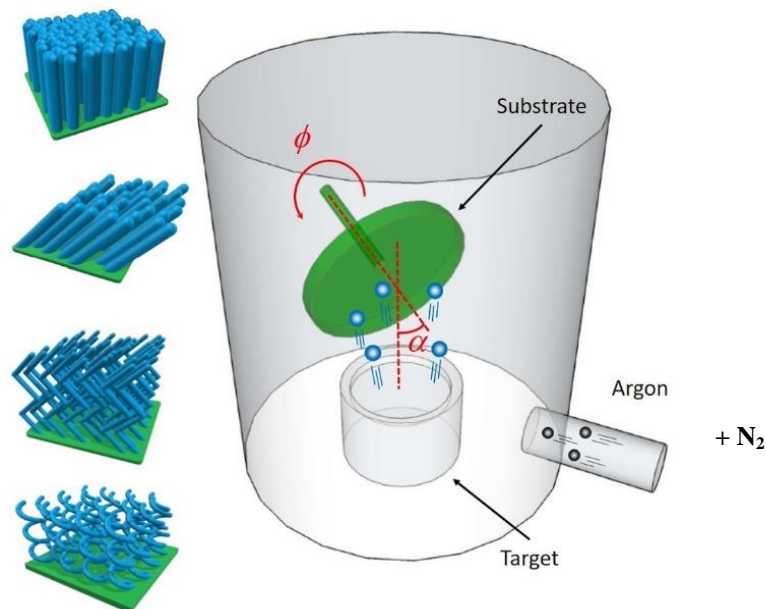


Figure 21 GLAD substrate holder technique used for TiN series.

Chemical and structural properties of TiN and (Ti,Al)N coatings with variation of structural design

The next observation relates to the progression of the films' composition, as shown in figure 22.

The ratio N/Ti rises as the tilting angle increases, illustrating the challenges the Ti atoms encounter in comparison to the nitrogen provided by the gas mixture inside the reactor in reaching the substrate.

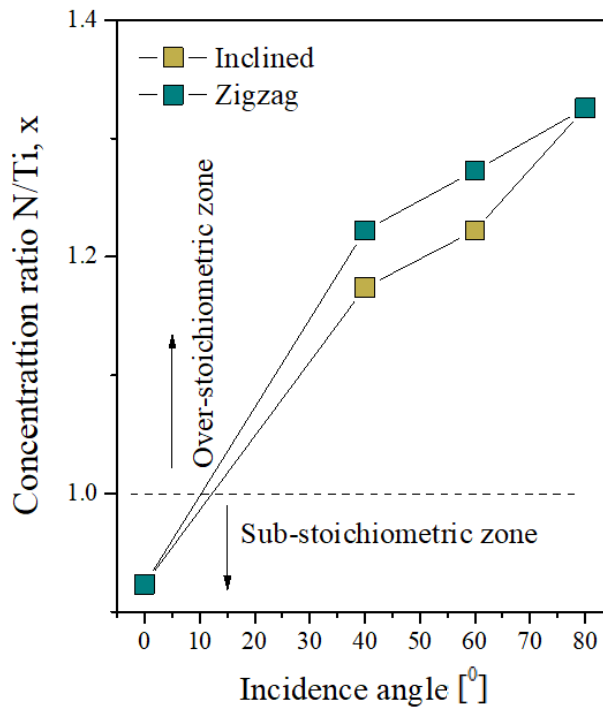


Figure 22 Evolution of Ti and N₂ concentration ratio, $x = CN/CTi$, in the sets of samples prepared in the tilted incidence series: inclined (series 1) and zigzag (series 2).

This result supports the tilting of the substrate's effects on the plasma atmosphere, as well as some discharge characteristics changes, such as the target's poisoning, which could explain why the target potential dropped toward lower values, similar to the over-stoichiometric samples prepared in the normal configuration (figure 22).

Figure 23 depicts the development of the two series of TiN samples that were created for this thesis' XRD diffraction patterns.

The inclined and zigzag coatings show crystal structures that are highly similar to one another (figure 23 (a, b)).

Figure 23 shows that the FCC TiN structure is constant throughout all of the produced samples and that the angular orientations of the diffraction patterns are essentially unaltered.

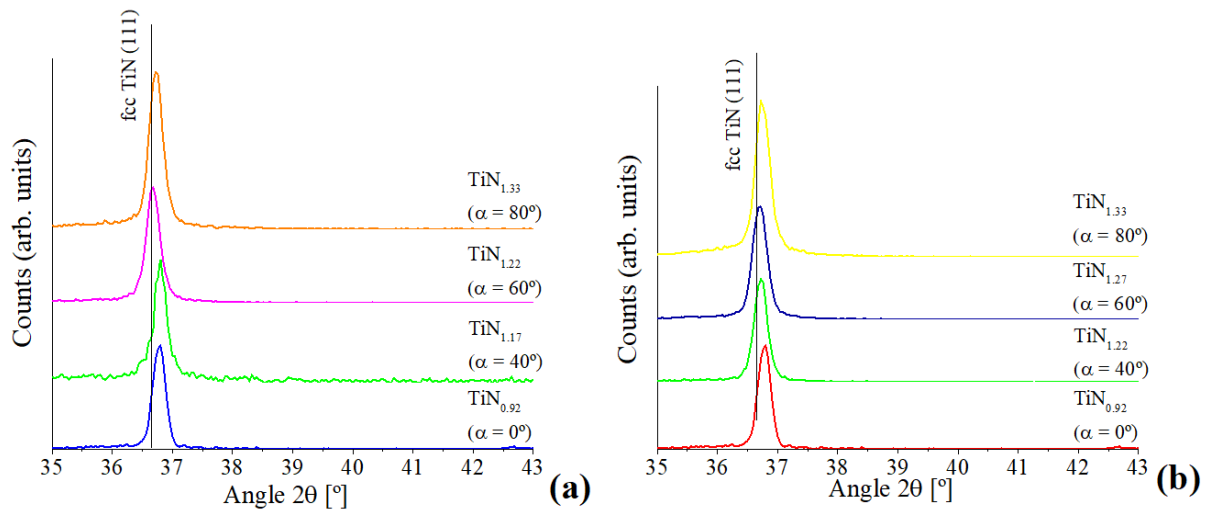


Figure 23 Evolution of the XRD patterns of the TiN_x thin films
(a) inclined geometry - series 1 and
(b) zigzag geometry - series 2.

The samples from these two series have similar structural characteristics, which is compatible with the fact that their composition only minimally varies (figure 22).

The tilted samples generated for ($\alpha = 60^0$ and 80^0), figure 23, appear to deviate to diffraction angles nearer to the FCC-TiN (111) structure, but there are only minor changes between them and the reference sample ($\alpha = 0^0$). The matching of the diffraction patterns also reveals some significant variances, particularly in terms of grain size evaluation (figure 24), in addition to the differential evolution of the diffraction patterns seen for the samples obtained in the different series. The first series has a dual behaviour as it follows the development of the diffraction patterns.

In comparison to the samples prepared under close- and over-stoichiometric settings, which display crystallites with diameters about 45 nm, samples prepared under sub-stoichiometric conditions (N/Ti atomic ratios obviously below 1) have smaller grain sizes (between 20 and 30 nm).

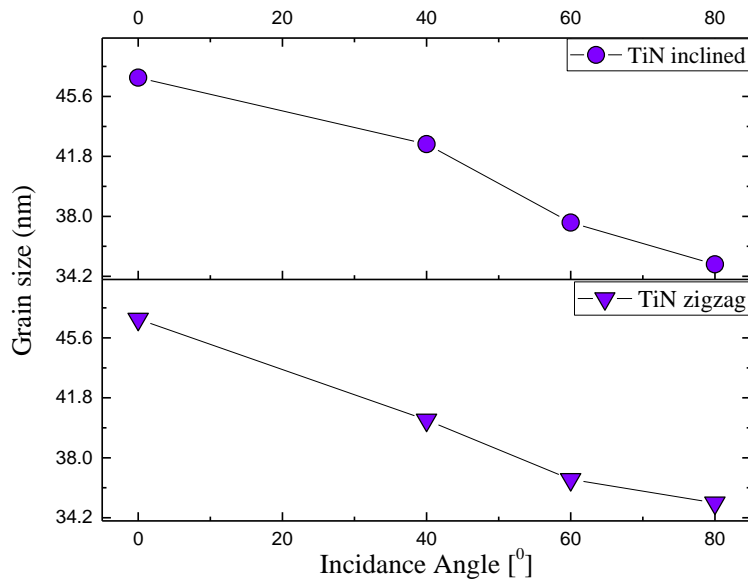


Figure 24 Evolution of grain size of the thin films prepared with tilted incidence angles in inclined (series 1) and zigzag (series 2) geometries.

The different grain size values are undoubtedly influenced by the target poisoning effect, the greater partial pressure of the gas atmosphere and the mobility and diffusion of the ad-particles driving the nanostructure evolution. Together with the declining tendency seen among the over-stoichiometric samples throughout the initial series, the grain size evolution is also clearly on the decline for the samples created with slanted nanostructures. The reduction of crystallites may be partially influenced by N/Ti atomic ratios of 1 or higher, but this effect must also be influenced by the increase in tilting angle, the shadowing effect and the lack of ad-particle diffusion once the particles have reached the substrate.

Morphological properties of TiN and (Ti,Al)N coatings with variation of structural design

Figures 25 (a-g) depict a slanted columnar structure having columns that are not separated from one another and are touching. This structure may be a direct result of shadowing effect and reduced thermalization degrees.

As a result of this logic, figures 25 (d) and (g) show that the films made with $\alpha = 80^\circ$, for both series, display - type microstructures including well and isolated inclined nano-columns.

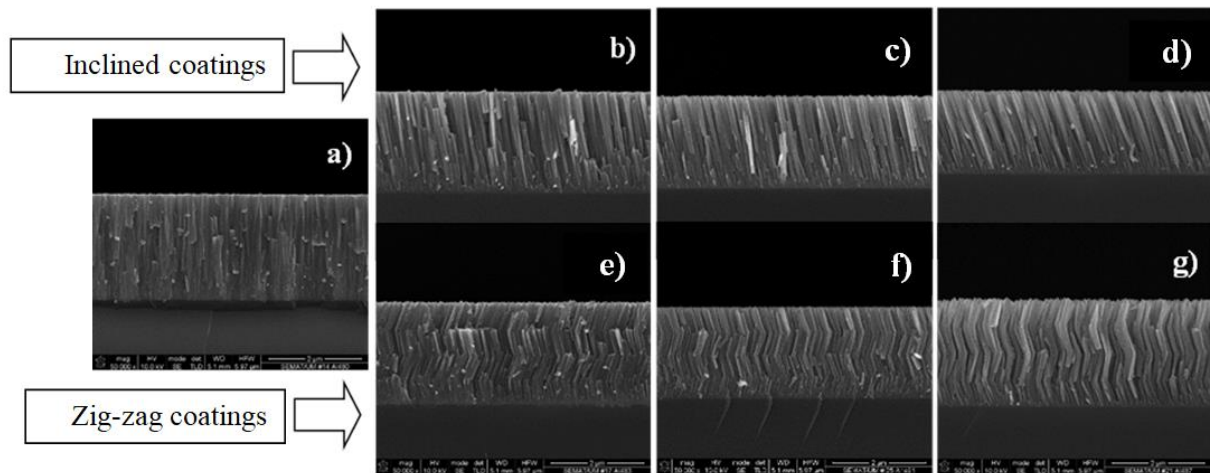
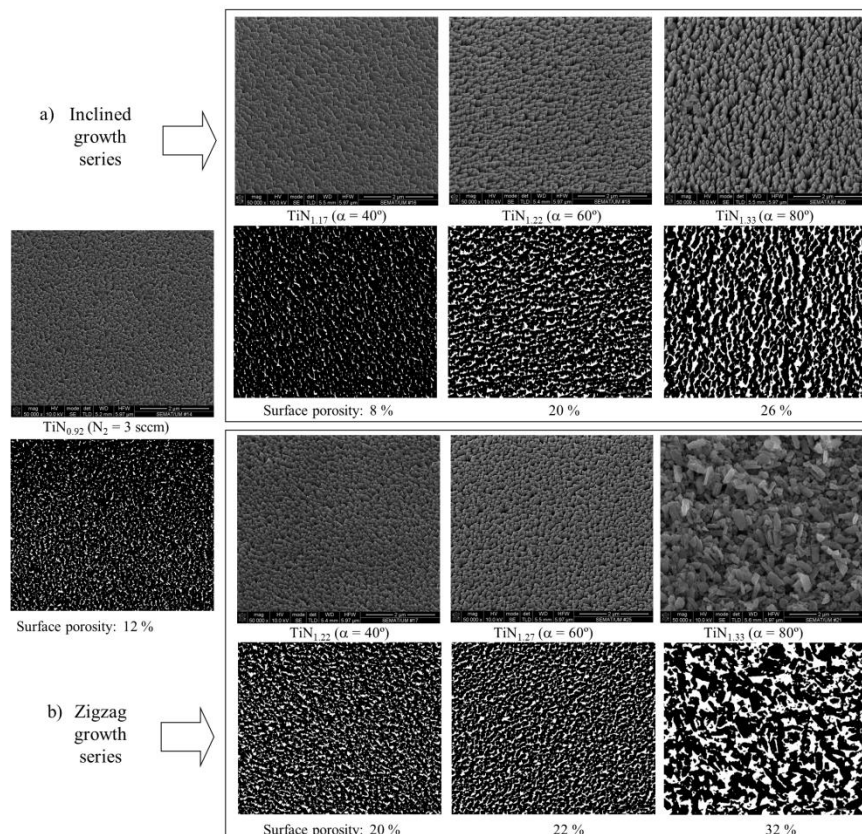


Figure 25 Cross-section SEM images of the two sets of samples: **(b-d)** TiN samples prepared with inclined geometry (incidence angles of 40° , 60° and 80°); **(e-g)** TiN samples prepared with zigzag nanostructured (incidence angles of 40° , 60° and 80°).

A MATLAB algorithm was used to analyze the surface porosity of every thin film microstructure, yielding binary pictures through a thresholding method. The results of the various growth morphologies indicated above are shown in figure 25, specifically in relation to the growth of surface finishing/defects as well as porosity (white regions in the surface pictures) (figure 26 (a, b)). In addition to the porosity estimates, the pores were examined, their Feret diameter distribution, pore count and average area are shown in figure 26 I. These findings demonstrate that changes in the microstructure are preceded by compositional and structural development, which, as will be demonstrated later in this thesis, will shape the thin film's reaction. The alterations in surface morphological characteristics for the samples created with different geometries, namely having either an inclined columnar design, or a zigzag nanostructure, stand out notably

for the samples made with the high tilting degrees ($\alpha = 60^\circ$ and 80°), which reveals extremely porous surfaces.

This behaviour is the consequence of shadowing effects and is compatible with the variations in the deposition parameters, especially the growth of the deposition rate as well as the indexed variations in composition and structural characteristics (figures 22 through 24). It's also important to take note of the adjustments made while designing nanostructures with tilted and zigzag geometries. Although, having equal deposition circumstances, the architectures created by the nanostructures of the films from both series with inclined and zigzag design, result in well-known structural and microstructural variations, such as changes in grain and pore diameters. In general and especially, the analysis of the histograms of the inclined and zigzag series (figure 26 I), demonstrates that in addition to the average pore size of the zigzag nanostructures always being greater than the value measured for tilted nano-columns (considering the same), the number of pores growing steeply with the inclination angle.



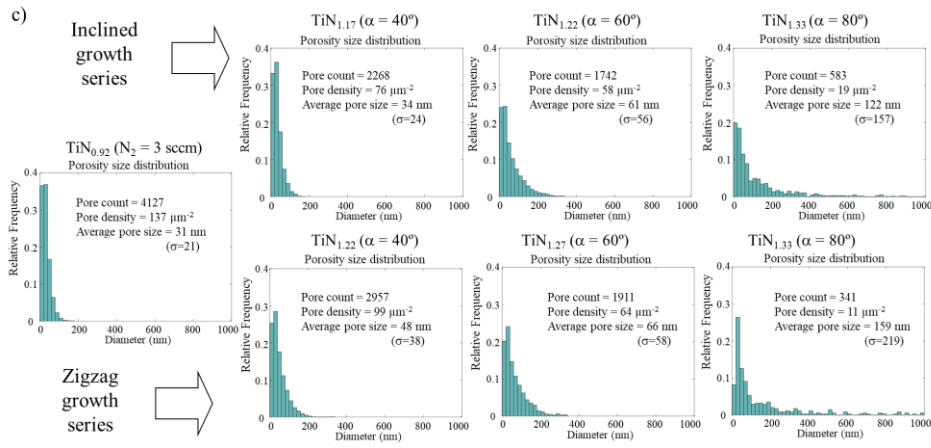


Figure 26 Top-view SEM micrographs of: **(a)** inclined incidence growth TiN samples and **(b)** zigzag incidence growth TiN samples; processed in MATLAB for surface porosity calculation and **I** corresponding histograms.

It is important to note that the samples created with the greatest tilt angles clearly show a rise in surface porosity and wider dispersion progression.

The greatest surface porosity is attained by the two samples created with the greatest tilt angle ($\alpha = 80^\circ$), as can be observed and both display a comparable variation trend that rises with the angle, α (figure 27).

Moreover, it is worthwhile to analyse a specific parameter that exhibits significant differences within each of the two sets of samples: the histogram analysis' measurement of the standard deviation of the distribution of pore diameters.

According to IUPAC's recommendations, the reference sample (deposited at normal incidence:

$\alpha = 0^\circ$ exhibits porosity values that can be classified as microporous-like (the pores are only a few nm in size), but as the incidence angle increases, there is a clear transition behaviour towards meso- and macro-porosity.

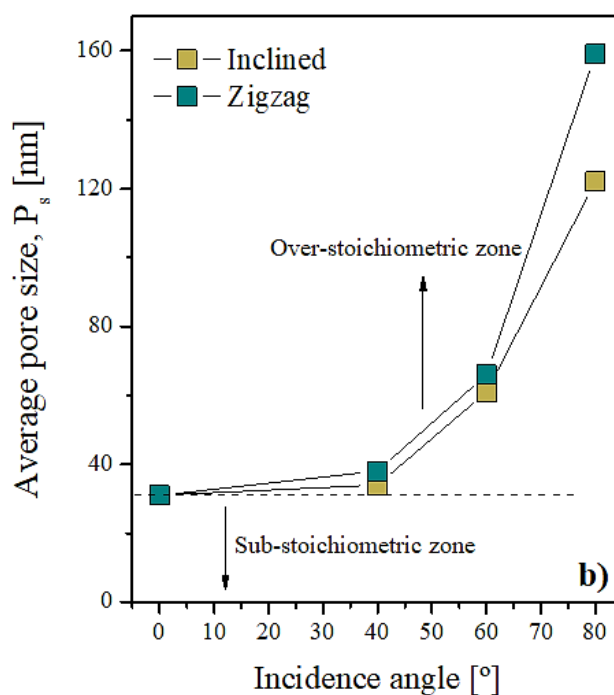


Figure 27 Evolution of the average surface pore size for the samples prepared in tilted incidence: inclined (series 1) and zigzag (series 2).

In contrast to the samples created with an incidence angle of 60° , which appear to show that the films are mostly mesoporous, but contain a considerable number of macro-pores, the samples deposited with incidence angle of 40° demonstrated little variations in comparison to the $\text{TiN}_{0.92}$ reference (width larger than 50 nm).

Although meso-porosity cannot be ignored, the thin films deposited with $\alpha = 80^\circ$ display bigger pores and may be loosely categorized as macro-porous. The surface morphology of the thin films is greatly influenced by the deposition angle, as seen in the preceding pictures.

The architecture and growth of the morphological characteristics were significantly influenced by the shadowing effects and discharge characteristics connected to the film's growth more than by the composition's actual evolution.

Atomic force microscopy (AFM), employing a high-resolution Nano-Observer AFM microscope (Concept Scientific Instruments), was used to examine the surface morphology of the films, including

roughness and porosity. Each sample was scanned with a 5 x 5 μm^2 area at a resolution of 1024 Px2 and a scan speed of 1 line/s. Figure 28 depicts the surface topography's development as determined by AFM. The variations resulting from increased incidence flux of the sputtered atoms are depicted in figure 29 as varied values of Root Mean Square (RMS) surface roughness. Figure 28 displays the various topographic patterns that the two TiN series have formed. Two very dissimilar behaviours can once again be observed, when the films made in inclined/ zigzag geometries (figures 28 (b, c)) are compared to the sample prepared in conventional geometry (figure 28 (a)).

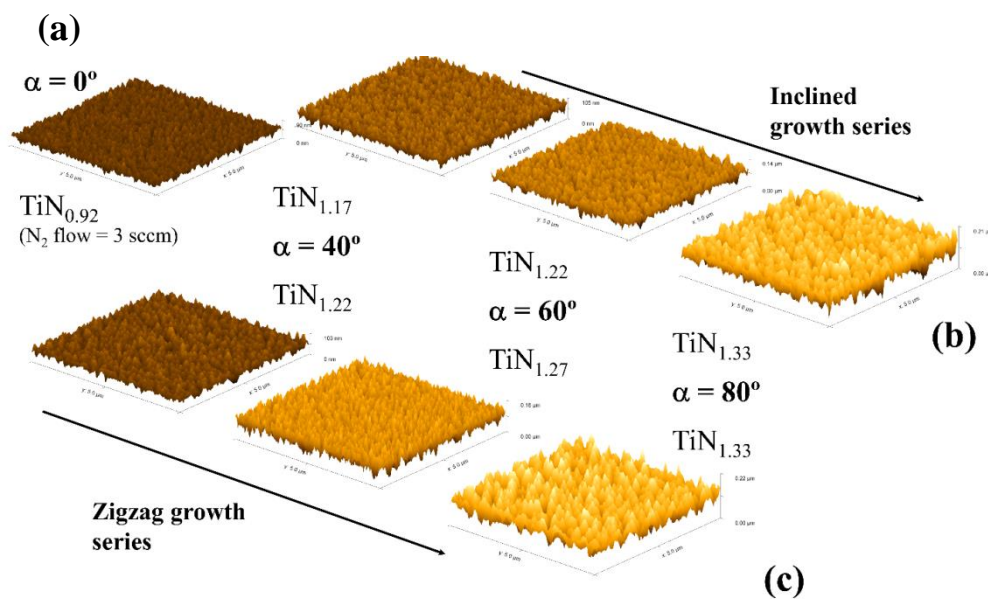


Figure 28 AFM scans of the three series of prepared samples in (a) normal columnar structure for reference, (b) inclined geometry and (c) zigzag geometry.

The findings demonstrate that conventional geometry film taken as a reference (normal incidence $\alpha = 0^\circ$) is much smoother and progressively rougher as the deposition angle increases.

A consideration for this behaviour is undoubtedly the impinging species' reduced penetration at tilted angles. Moreover, a significant portion of the energy deposited by atoms colliding at glancing angles is transferred to surface atoms, increasing atom mobility. Sputtering is presumably to blame for some of the roughening brought on by glancing angle bombardment.

The two TiN series created with a tilted incidence angle become rougher as the deposition angle is more oblique due to the more porous surfaces and less dense structures. According to the RMS values shown in figures 29 (a,b), the inclined films deposited at an angle of $\alpha = 80^\circ$ film with tilted nano-columns is twice as rough as the TiN reference sample ($\alpha = 0^\circ$). The set of findings shown in figures 25 through 28 demonstrate once more that it is possible to customize the microstructure and surface characteristics of a specific thin film system simply by acting on the growth design while also taking into account the fact that all the samples were made with nearly identical deposition parameters (thickness, target current).

For the majority of technical and industrial applications, including the biomedical sector for cellular growth enhancement/adhesion, chemical and physical sensing, mechanical and tribological applications, among many others, the tailoring of the surface roughness and the sort of columnar growth is of utmost importance. The final point concerns a comparison of the grain size progression trends of the samples (figure 24) and the surface roughness values (figure 29), which also takes into account variations in the average pore diameters (figure 27).

The series prepared with tilted angles have a completely different behaviour from the reference sample where $\alpha = 0^\circ$.

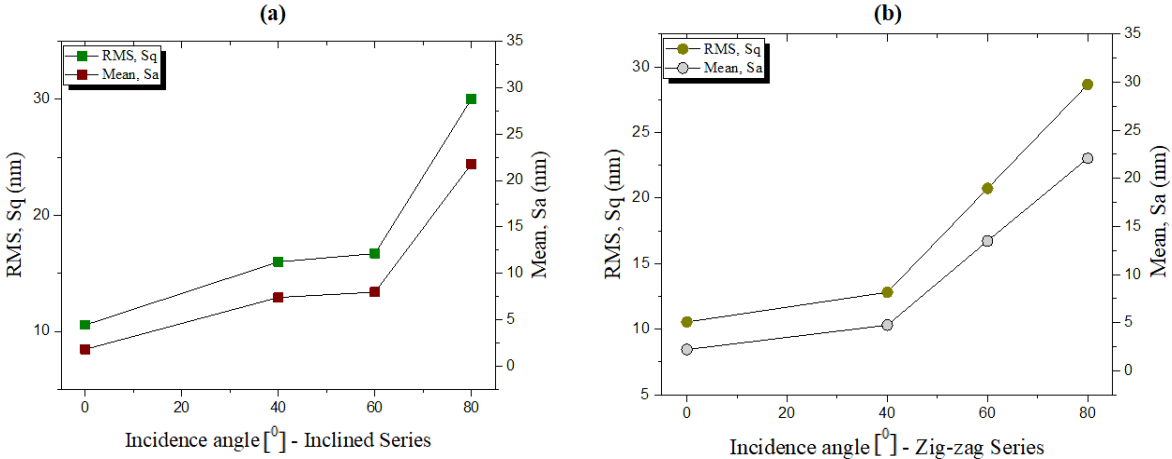


Figure 29 Evolution of the surface roughness values of the two TiN series; (a) inclined nano-columns and (b) zigzag nanostructures incidence.

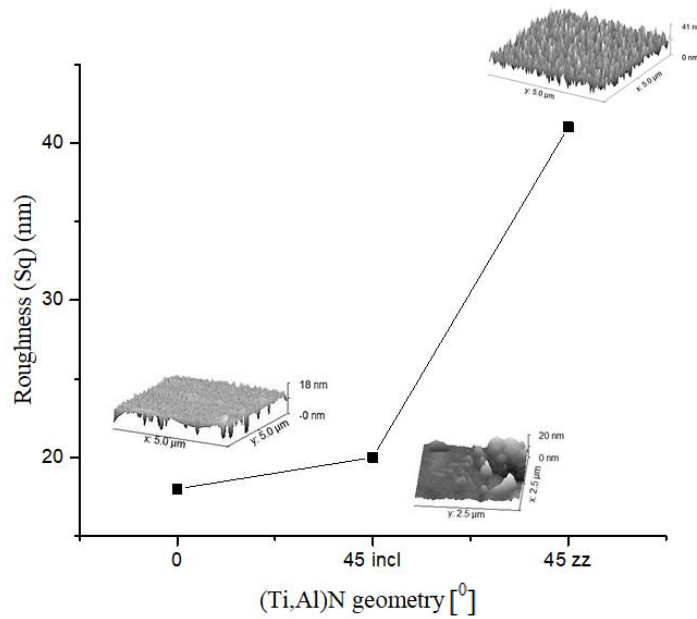


Figure 30 Evolution of the surface roughness values of the (Ti,Al)N coatings with different nanostructured design.

On the other hand, the roughness of (Ti,Al)N coatings increases when the structure changes from a normal columnar structure to a 45° inclined and zigzag nanostructured design due to the increased complexity and irregularity in the surface morphology (figure 30).

The inclined and zigzag structures create more pronounced surface features and variations, leading to higher surface roughness compared to the relatively uniform and smoother normal columnar structure.

Thermal properties of TiN and (Ti,Al)N coatings with variation of structural design

Figure 31 displays the results of direct measurements made on the various collections of samples. The results for the thermal diffusivity, which were in the $10^{-6} \text{ m}^2\text{s}^{-1}$ range for all samples from the two series, agree with earlier findings for Ti films, demonstrating that the distinctive geometries do not significantly alter the thermal properties but can instigate a

distinct trend that can be helpful when modifying the properties of materials.

Though the case, it is clear that the thermal diffusivity and thermal effusivity both drop as the incidence angle rises, regardless of the design that is chosen. In conclusion, the films' thermal conductivity likewise declines in line with the general trend.

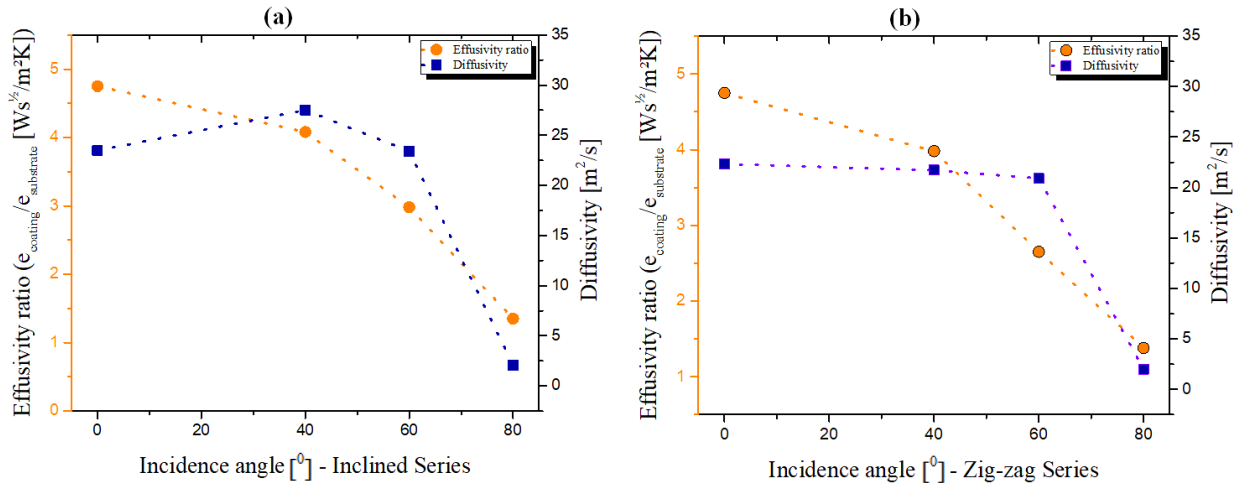


Figure 31 Evolution of the effusivity ratios and the diffusivity values for the samples prepared:

(a) prepared with tilted angles in inclined geometry and

(b) zigzag geometry.

Optical properties of TiN and (Ti,Al)N coatings with variation of structural design

The optical characteristics of the two series of thin films demonstrate significant evolution tendencies in addition to changes in composition, morphological and structural aspects, as shown in figure 32. The values of reflectivity for the two sets of samples prepared with inclined and zigzag geometries are shown in figure and they significantly differ from the reference coating with a normal columnar growth ($\alpha = 0^0$). This difference can be attributed to multiple photon scattering on the rougher surfaces of the samples prepared with greater incidence angles (figure 28 (b,c)).

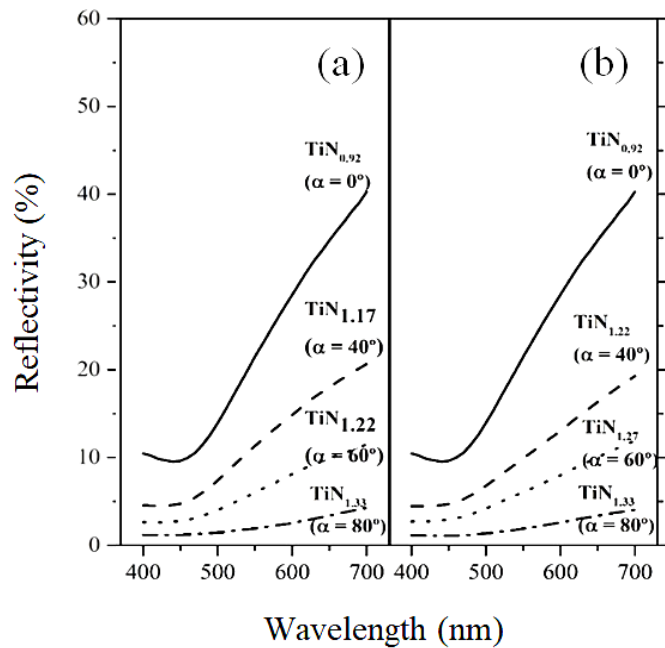


Figure 32 Evolution of the reflectivity of:
(a) TiN thin films prepared with tilted angles and
(b) TiN coatings with zigzag geometry.

Many light reflections occur on the surface as a result of the RMS surface roughness's substantial rise (figure 29). Moreover, the relatively rough surfaces increase the amount of electron scattering at the Fermi surface, which causes scattering loss. Scattering loss is also the reason for the decrease in reflection intensity and, thus, a decrease in the sample's reflectivity. Non-specular scattering also appears in these samples processed at tilted angles due to an increase in surface roughness (observed in the measurements).

The evolution of the films' colour coordinates, shown in figure 33, follows the changes in reflectivity and exhibits a similar evolution pattern.

It is feasible to see a considerable shift in the optical behaviour for the two sets of samples that were manufactured at tilted angles (figure 33), with a systematic drop for all the colour coordinates. The samples' deterioration, ranging from golden to dark brownish tones, is apparent as the incidence angle increases.

Together with the samples' darkening, the yellow and blue coordinate (b^*) falls dramatically as well (bluish). The modest drop in the red and green coordinate (a^*) indicates a propensity for reddish tones.

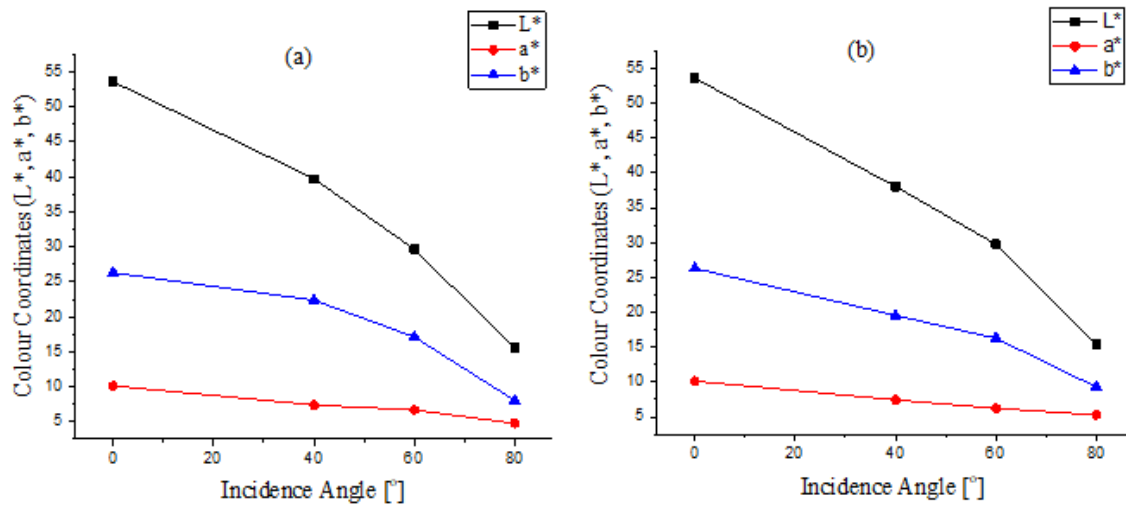


Figure 33 Evolution of the colour coordinates of the thin films:
(a) prepared with inclined geometry and
(b) zigzag geometry.

The evolution of colour coordinates as a function of the deposition parameters, seen in figure 33 and represented by the so-called colour difference parameter, E^* , is a last intriguing aspect. When comparing two samples' colour coordinate evolution, it is possible to detect small deviations even when they first appear to be comparable. To assess a sample's surface quality and suitability for a particular application, it is essential to compare it to a reference sample that has a similar colour to the sample in question.

The most intriguing aspect is the large fluctuation in E^* for the samples created at tilted angles of 60° and 80° (from both series), which almost doubles and triples the outcome for the sample prepared at $\alpha = 40^\circ$ figure 34. These outcomes confirm the significant variations identified for the surface features of the samples in the preceding sections, even after accounting for the consistency of the deposition parameters employed in order to prepare the two series with tilted angles (the same

thickness, nitrogen and argon flows). Despite the modest compositional variations, the film's nanostructure design was specifically tailored to allow for large variations in colour tones, as seen in figure 34.

The greatest variations in optical responses are found in the two series prepared at tilted angles, highlighting the main role of the morphology, specifically the surface roughness and porosity brought about by the film growth processes.

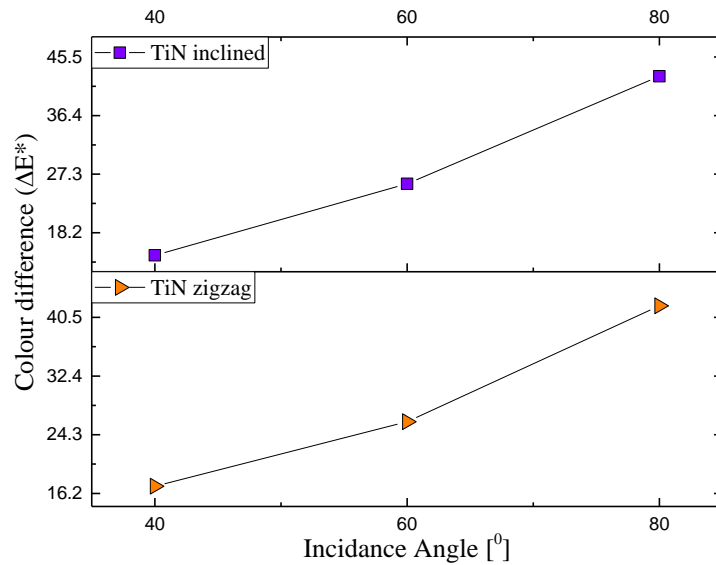


Figure 34 Evolution of the colour difference for the thin films prepared with inclined geometry and zigzag geometry.

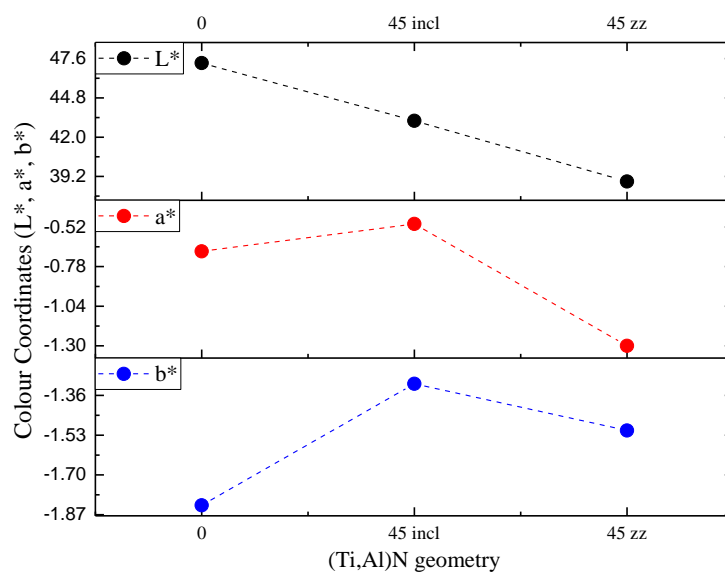


Figure 35 Evolution of the colour coordinates of (Ti,Al)N thin films with different nanostructured design.

The increase in surface roughness as a consequence of changed (Ti,Al)N nanostructured designed coating (from normal columnar structure to inclined and zigzag designs) results in a greater scattering of light, leading to a darker appearance.

In the L^* , a^* , b^* colour coordinate system, this increased roughness decreases the L^* value (lightness), making the coating appear darker. The irregular surface morphology creates more shadows and absorbs more light, further reducing reflectivity and contributing to the darker optical appearance (figure 35).

Electrical properties of TiN and (Ti,Al)N coatings with variation of structural design

For every one of the two sets of samples, figure 36 depicts the development of the thin films' resistivity.

The films created in the inclined and zigzag series, similarly to the evolution of optical responses, show an amplitude of variation of almost three orders of magnitude, which is much greater than what was seen for the films created in the conventional geometry, where the resistivity values increased below one order of magnitude, highlighting once more the predominance of morphological features over composition and structural changes.

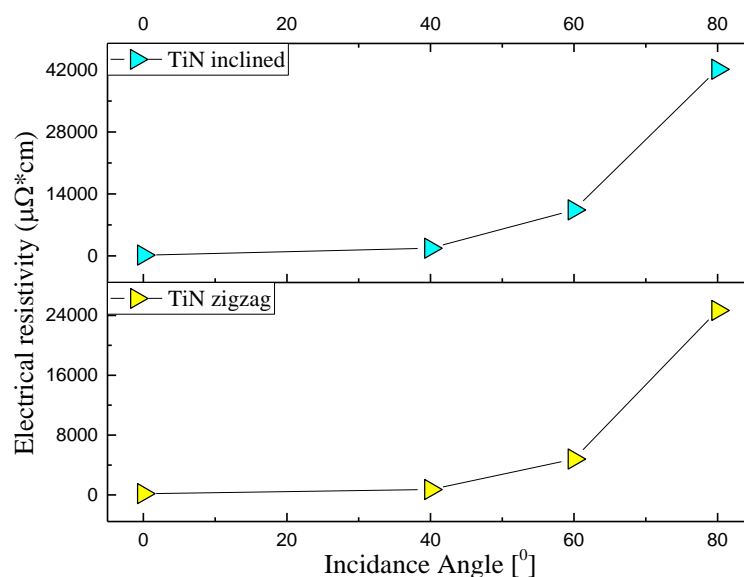


Figure 36 Evolution of the electrical resistivity of the thin films prepared with inclined- and zigzag geometry.

Despite the increase in crystallite sizes in this zone, the influence of the scattering effects by the surface roughness features seems to be the major parameter to take into consideration for this fluctuation.

Mechanical and tribological properties of TiN and (Ti,Al)N coatings with variation of structural design

Figure 37 shows the evolution of the hardness and elastic modulus values for the two set of samples of TiN coatings prepared in inclined nano-columns and zigzag nanostructures incidence.

For comparative purposes, the first value in the graph represents the sample with a normal, columnar growth.

The hardness and Young's modulus of TiN coatings decrease when the deposition angle changes from 0° (normal incidence) to higher angles ($\alpha = 40^\circ, 60^\circ, 80^\circ$) due to several reasons related to the microstructure, density, and film growth mechanisms influenced by the deposition angle.

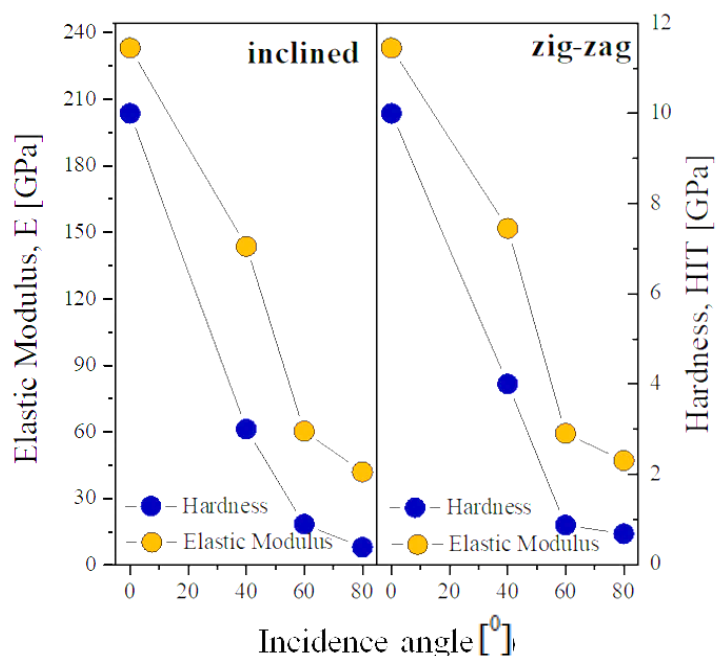


Figure 37 Evolution of the hardness and elastic modulus values for the three series of TiN sample prepared in inclined nano-columns and zigzag nanostructures incidence.

As the deposition angle increases, the shadowing effect becomes more pronounced. This leads to the growth of a more porous, columnar structure because the incoming flux of depositing atoms has a more oblique trajectory, causing atoms to shadow each other and creating voids between the columns.

The increased porosity results in a lower density of the coating. Lower density coatings have reduced mechanical integrity, leading to lower hardness and Young's modulus. Moreover, the bonding between tilted columns is typically weaker compared to vertically aligned columns, leading to easier deformation and reduced hardness and modulus.

Additionally, changes in crystallographic texture and reduced adatom mobility at higher angles contribute to the decrease in hardness and modulus. The same tendency of decreasing is seen in both series, inclined and zigzag structured coatings (figure 37).

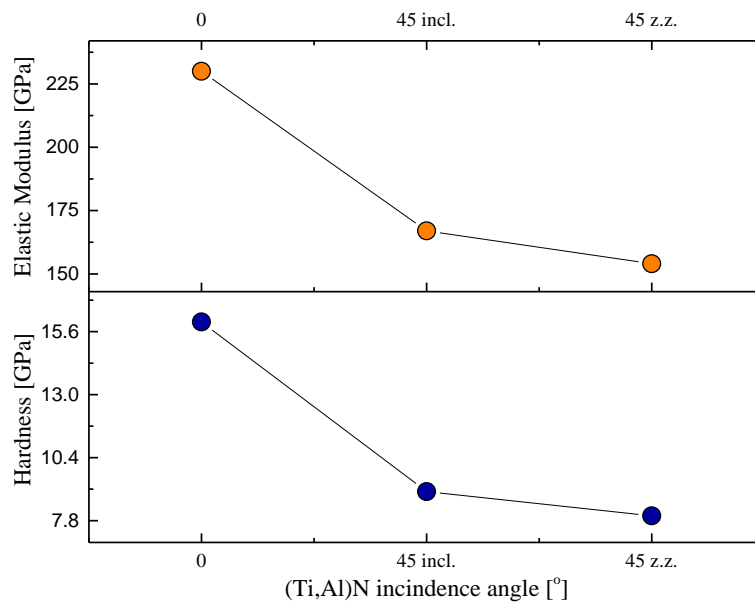


Figure 38 Evolution of the hardness and elastic modulus values for the (Ti,Al)N samples prepared with normal incidence angle, inclined nano-columns and zigzag nanostructured designs.

The decrease in hardness and elastic modulus of (Ti,Al)N coatings, presented in figure 38, when the nanostructure changes from normal to inclined and zigzag structures is mainly due to

increased porosity, higher residual stress and a less favorable crystallographic orientation.

These changes lead to a less dense microstructure with more defects, making the coating weaker and more prone to deformation under load. Further, the zigzag structure introduces additional interfaces and boundaries within the coating.

While zigzag nanostructured coatings can sometimes impede crack propagation, they can also act as weak points for deformation, especially under shear stress.

Another crucial parameter is the ratio H^3/E^2 , which represents the capacity of the material to disperse energy at plastic deformation during loading. When the H^3/E^2 ratio has higher values, it indicates a good balance of hardness and elasticity, enhancing durability and reducing crackings or delaminations. The toughness values represented by this ratio is a valuable indicator of mechanical performance of TiN and (Ti,Al)N hard coatings.

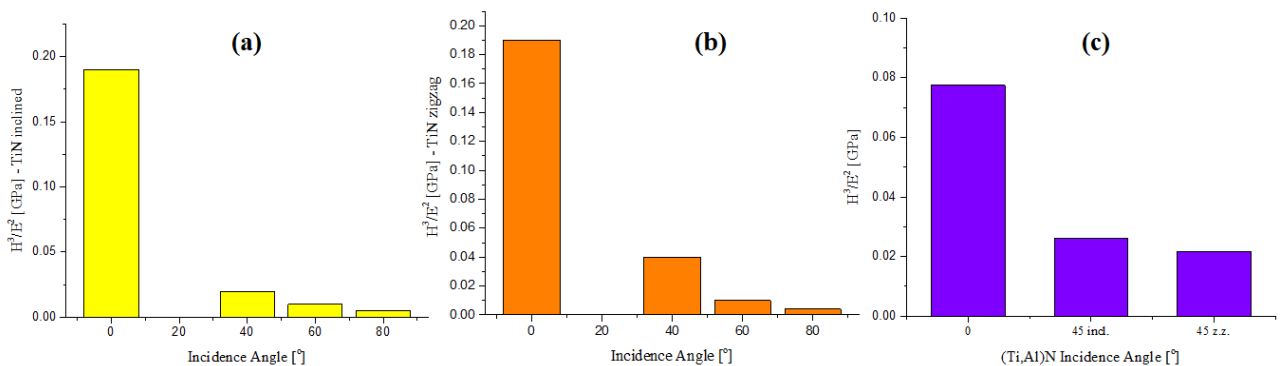


Figure 39 Evolution of H^3/E^2 ratio of: **(a)** TiN coatings with inclined nanostructural design; **(b)** TiN thin films having a zigzag structure; **(c)** (Ti,Al)N coatings with normal incidence ($\alpha = 0^\circ$), with inclined columnar growth and with zigzag nanostructure.

The H^3/E^2 ratio decreases in TiN coatings when changing the nanostructural design from a normal incidence angle to 40° , 60°

and 80° inclinations and to zigzag structures using the same angles ($\alpha = 40^\circ, 60^\circ, \text{ and } 80^\circ$) due to increased surface roughness, which reduces hardness and stiffness (figure 39 (a,b)).

This decrease of the ratio indicates a reduced resistance to plastic deformation and wear.

The complex nanostructures often lead to higher surface roughness and weaker bonding, reducing the overall hardness and stiffness of the coating.

This is the case also for (Ti,Al)N coatings. As the nanostructure changes from normal columnar structure to inclined and zigzag nanostructure, the balance between hardness and elasticity deteriorates, resulting in a lower H^3/E^2 ratio and decreased resistance to plastic deformation and wear (figure 39).

After the hardness, elastic modulus and the H^3/E^2 ratio were calculated, the research proceed with the adhesion characterization, where a Poisson ratio value of 0.25 was used for all the investigated TiN and (Ti,Al)N thin films.

In order to determinate the values of the critical loads and friction coefficient, linear scratch tests (5 different scratches), with progressive loads up to 30 N, were performed using the following test parameters: loading rate of 3 N/min, scratch length of 5mm and scratch rate of 2.5 mm/min.

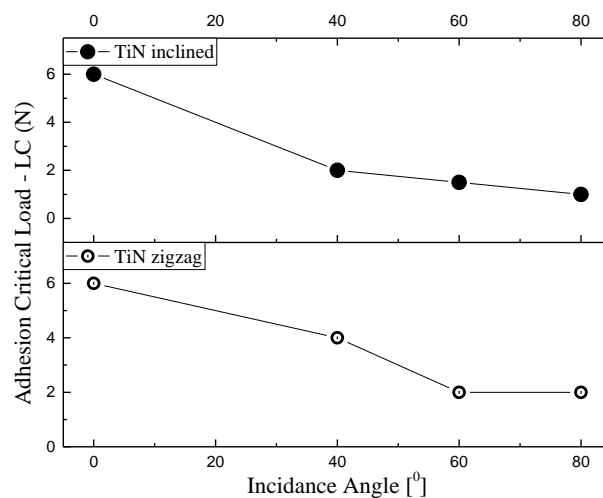


Figure 40 Critical load of adherence (L_{C3}) variation of TiN coatings for inclined and zigzag nanostructures.

The adhesion critical load of TiN coatings decreases with increasing deposition angles due to the formation of a more porous and less dense columnar microstructure, which weakens the mechanical integrity of the coating (figure 40).

Higher deposition angles introduce more defects, such as voids and microcracks and result in pronounced grain boundaries that act as points of mechanical weakness. The inclined deposition also leads to suboptimal bonding between the coating and substrate, reducing the effective atomic packing and contact area, which compromises adhesion strength. Additionally, increased residual stresses and surface roughness at higher angles further diminish the mechanical interlocking and cohesive strength of the coating. As consequence, these factors collectively contribute to a lower critical load required for adhesion failure, making the coating more susceptible to delamination.

The adhesion critical load (L_{C3}) decreases in (Ti,Al)N coatings when transitioning from a normal incidence angle to a 45 degree inclination and further to a zigzag nanostructure due to increased internal stresses and defects in the more complex structures (figure 41).

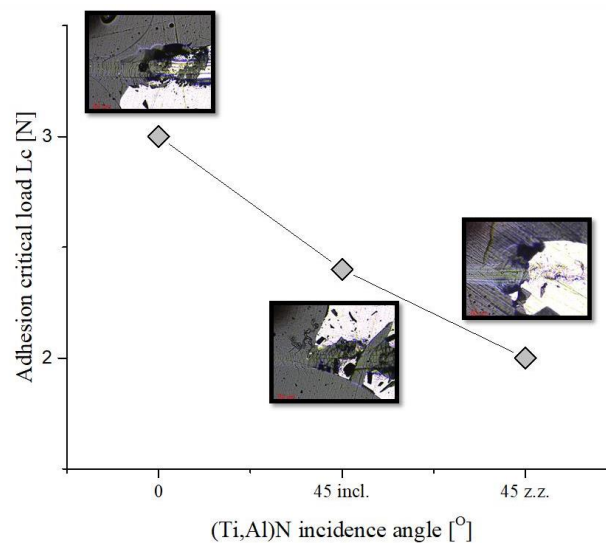


Figure 41 Critical load of adherence (L_{C3}) variation for (Ti,Al)N coatings with inclined and zigzag nanostructure.

These structural changes lead to higher surface roughness, which induces stress concentrations at the interface, weakening adhesion. Additionally, the effective contact area is reduced in inclined and zigzag structures, further compromising adhesion strength. Consequently, the overall integrity and adhesion of the coating diminish with increased structural complexity as it is shown in figure 41.

The tilted columnar growth at higher deposition angles results in anisotropic mechanical properties, where certain directions of sliding may encounter higher resistance due to the orientation of the columns and grain boundaries, thus increasing the friction coefficient. The friction coefficient of TiN coatings increases with higher deposition angles for both series, inclined and zigzag nanostructured coatings, due to elevated surface roughness and the formation of a higher porous, columnar microstructure (figure 42). Increased porosity and defect density create a less uniform surface, enhancing abrasive interactions with the counter surface.

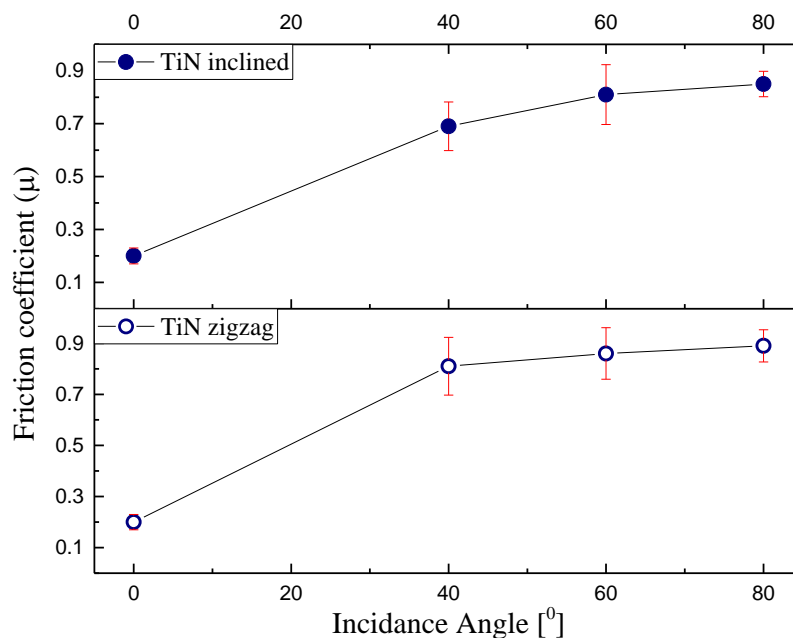


Figure 42 The variation of dynamic friction coefficient of TiN series for the inclined and zigzag nanostructured coatings.

Pronounced and weaker grain boundaries at higher angles contribute to increased microscale friction as grains deform or dislodge more easily.

Overall, these factors reduce the effective lubricity of the coating, resulting in increased friction (figure 42).

After the friction coefficient was determined, the wear rate of both series, with inclined columnar growth and with zigzag like structure, was calculated.

Figure 43 presents an increase in the friction coefficient when the nanostructured (Ti,Al)N coatings change from normal incidence to 45° inclination and to a zigzag structure due to increased surface roughness, which enhances mechanical interlocking and frictional resistance.

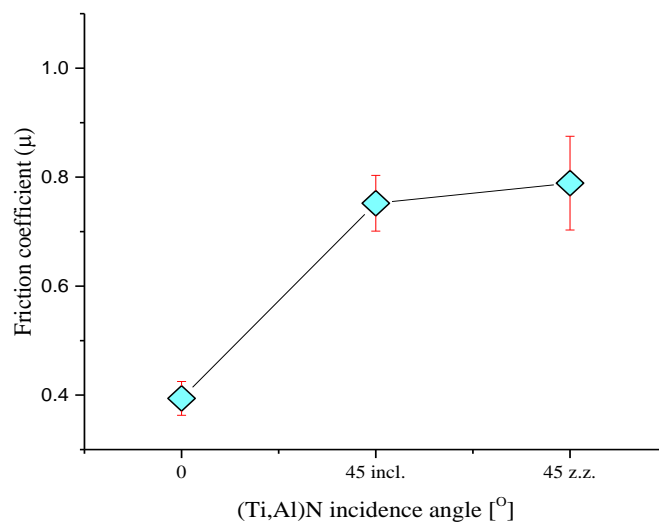


Figure 43 The variation of dynamic friction coefficient of (Ti,Al)N set of samples for the inclined and zigzag nanostructured coatings.

Additionally, these more complex structures create a larger effective contact area with more contact points, leading to higher friction.

The intricate nanostructures also cause greater material deformation and delamination during sliding, contributing further to the increased friction coefficient.

In figure 44 it can be observed an increase in the tendency regarding the wear rate of both TiN nanostructured designed coatings.

An increased wear rate compromises the durability, performance and reliability of coated components, leading to higher maintenance costs and potential operational risks.

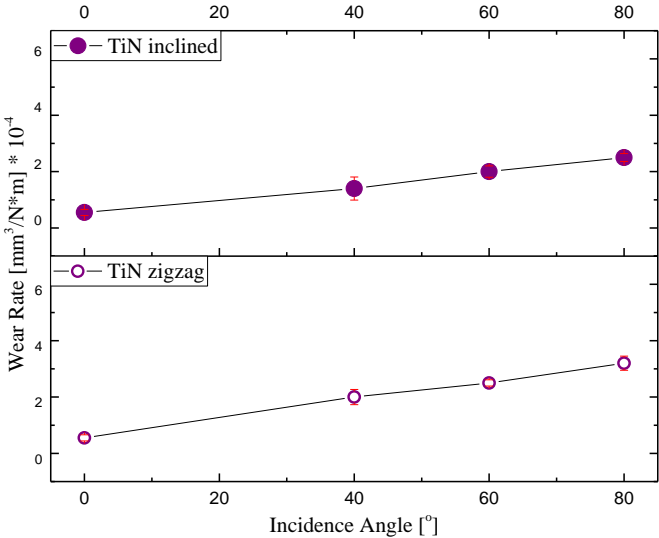


Figure 44 Evolution of wear rate of TiN coatings for inclined and zigzag depositions.

In figure 45, the wear rate increases when the nanostructure of (Ti,Al)N coatings changes from a normal incidence angle to a 45° inclination and zigzag nanostructured design due to higher surface roughness, which enhances abrasive interactions. The more complex structures also have weaker structural integrity, leading to greater susceptibility to wear.

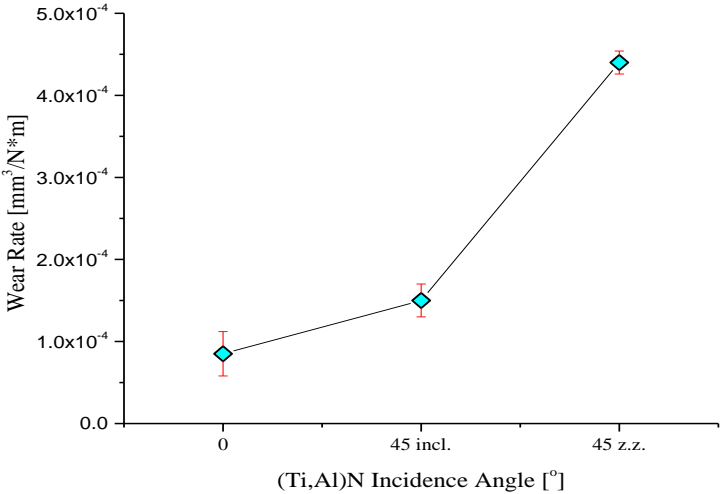


Figure 45 The evolution of wear rate of (Ti,Al)N coatings for inclined and zigzag depositions.

Additionally, the higher friction coefficient in these structures, results in increased energy dissipation as heat and mechanical deformation, accelerating material removal. Therefore, increased friction directly contributes to a higher wear rate in these coatings.

Corrosion behaviour of TiN and (Ti,Al)N coatings with variation of structural design

Figure 46 shows the evolution of OCP for the last 10 min of immersion and representative potentiodynamic polarization curves of all thin films obtained in 35 g/L NaCl solution at room temperature. The corrosion parameters such as open circuit potential (E_{OCP}), corrosion potential ($E_{(i=0)}$), passivation and corrosion current densities (i_{pass} and i_{corr}) are presented in Table 1. Through OCP evolution it is possible to observe that all groups of samples presented a stable behaviour.

The recorded OCP values were nobler for both sets prepared with inclined and zigzag-like geometries than for the close stoichiometric $\text{TiN}_{0.92}$ reference film, which indicates a lower tendency to corrosion for the films growing in inclined geometries.

For the two set of samples, prepared with inclined and zigzag geometries, the potentiodynamic polarization curves did not present a clear passivation plateau and the curves are shifted to higher values of current densities (figure 46).

Although no passivation plateau was observed, it might be assumed that the tilted incidence series of samples exhibit a passivation region, which is characterised by a slow increase of the current densities on the anodic domain. This behaviour can be attributed to the heterogeneities of the passive film formed inside the thin columns.

In addition, even though the increased surface porosity of these architected thin films might facilitate the electrolyte penetration through the columns, the difficulty of the oxygen diffusion might lead to a difference in the thickness and the

nature of the passive film (oxide film). Also, the formation rate of the passive film might be different inside the columns considering the different average pore sizes detected for each thin film prepared in this group ($\alpha \geq 40^\circ$).

The corrosion kinetics was accessed by i_{corr} , where the two sets of samples presented higher values of i_{corr} than the stoichiometric $\text{TiN}_{0.92}$ thin film with conventional geometry, used as reference. The lack of a well-defined passivation plateau and higher corrosion kinetics for the thin films prepared with inclined and zigzag geometries can be attributed to the heterogeneities, such as porosity or roughness.

Besides, these samples presented well-defined columnar growth, with thinner, but compact columnar aggregation, which may explain the similar corrosion rate of the inclined samples with $\alpha = 60^\circ$ and $\alpha = 80^\circ$ and zigzag with $\alpha = 60^\circ$.

However, for the zigzag-like samples prepared with $\alpha = 80^\circ$, the corrosion resistance significantly decreases.

In fact, this set of samples was the one that presented the highest average pore size (160 nm for $\alpha = 80^\circ$), which facilitates the penetration of the electrolyte and thus allows an acceleration of the corrosion mechanisms.

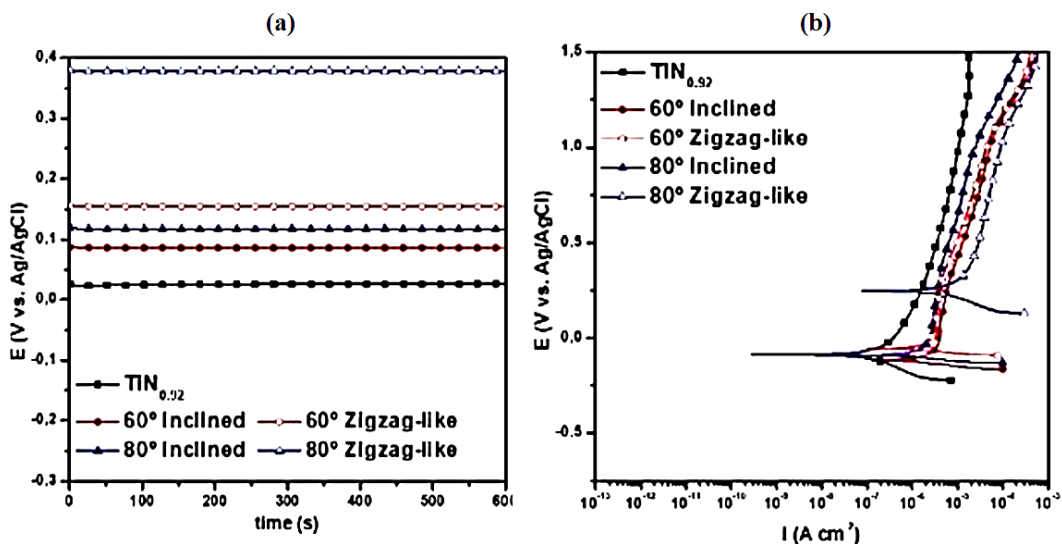


Figure 46 (a) OCP evolution for the last 10 min of immersion and (b) the representative potentiodynamic polarization curves for inclined and zigzag-like geometries, respectively.

Table 1. Open circuit potential (E_{OCP}), corrosion potential ($E_{(i=0)}$), passivation current density and corrosion current density values for inclined and zigzag nanostructured thin films:

| Samples | E_{OCP} [V _{Ag/AgCl}] | $E_{(i=0)}$ [V _{Ag/AgCl}] | i_{corr} [$\mu A\ cm^{-2}$] |
|---------------------|--------------------------------------|--|------------------------------------|
| TiN _{0.92} | 0.060 ± 0.051 | -0.057 ± 0.055 | 0.22 ± 0.01 |
| TiN 60°_Inclined | 0.097 ± 0.020 | -0.111 ± 0.46 | 1.46 ± 0.12 |
| TiN 60°_ZigZag | -0.037 ± 0.045 | -0.035 ± 0.045 | 1.28 ± 0.11 |
| TiN 80°_Inclined | 0.158 ± 0.036 | -0.060 ± 0.041 | 1.22 ± 0.38 |
| TiN 80°_ZigZag | 0.262 ± 0.190 | 0.129 ± 0.152 | 7.27 ± 3.66 |

When the phase angle approaches -90° , for middle and low frequencies range, describes the typical capacitive response of the passive film formed on the thin film surface, in other words, as close to -90° the phase angle better quality of the passive film. Figure 47 represents the EEC for the TiN_{0.92} with non-conventional geometries, representing the formation of a passive film both on the outmost surface and inside of the thin film columns. Since these oxides films have different nature and quality, it must be considered that these oxide films have their own resistance and capacitance. Thus, it was presumed that the surface oxide film is more protective than the oxide film formed inside the pores hence its resistance may be considered as too high to be included in the model.

Therefore, the resistance element corresponding to Q_1 was not included in the circuit due to its insulating behaviour. An additional electrolyte resistance (R_1) was added to the EEC as the electrolyte contribution inside the thin films' columns.

However, once the oxide film inside of the column is less protective, its resistance (R_2) should be considered in the EEC model. Consequently, the pair (R_2/Q_2) was added to the EEC.

In ECC, a CPE was used instead of capacitor to fit the EIS results, once this element allows the representation of a non-ideal capacitor. A non-ideal capacitor is described when $n \approx 1$, where this element is influenced by the surface roughness and its heterogeneities. The EEC parameters obtained from EIS data are presented in Table 2. $TiN_{0.92}$ thin films presented lower Q_1 values as compared with non-conventional geometry thin films, indicating that the passive film formed on their surface is less protective. However, within the non-conventional geometry thin films no significant differences on Q_1 values were found, thus, it can be said that the passive film formed on the surface had similar protective properties. Considering the Q_2 values, the lowest value was found to be for $TiN_{0.92}$ with $\alpha = 80^\circ$ inclined, between the $TiN_{0.92}$ obtained at 60° with both geometries (inclined and zigzag) no significant differences were observed and $TiN_{0.92}$ having $\alpha = 80^\circ$ zigzag presented the highest value of Q_2 . Therefore, these results suggested that the increase on the porosity led to less protective passive film. This behaviour may be connected to the difficulty of the electrolyte fill the columns, leading to a slower the growth of the protective passive film which may also lead to formation of heterogeneous film mainly of its thickness.

In figure 47, the resistance of the passive film on TiN thin films, obtained from EIS results is shown. This resistance can be referred as polarization resistance, which is an electrochemical parameter inversely proportional to the corrosion rate (i_{corr}). The corrosion current density, Q_1 and Q_2 values, obtained from potentiodynamic polarization curves and

EIS results, respectively, of all $\text{TiN}_{0.92}$ thin films are presented in figure 47.

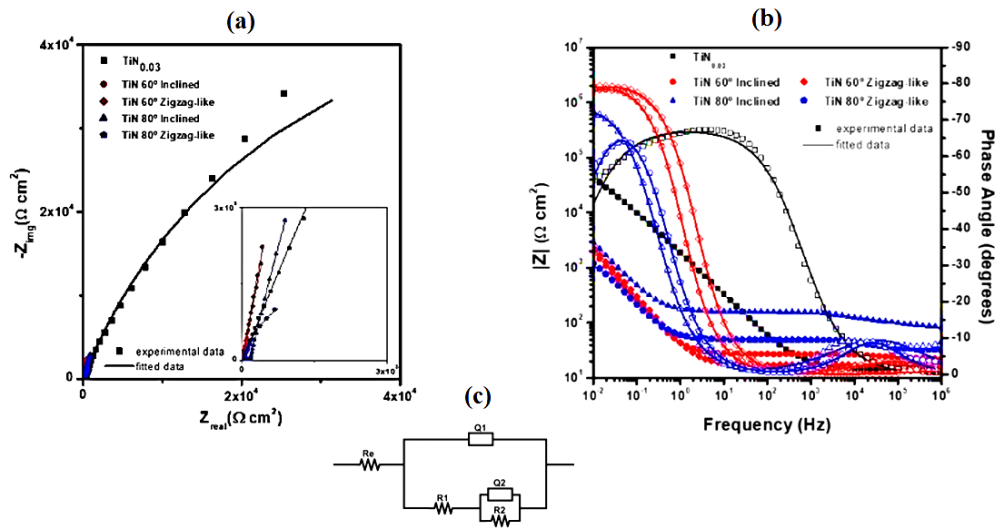


Figure 47 EIS spectra in form of (a) Nyquist and (b) Bode diagrams for thin films with inclined and zigzag-like geometries, respectively, together with EEC used to fit EIS results.

Table 2. EIS parameters obtained by fitting with the proposed ECC.

| Samples | Re [$\Omega \text{ cm}^2$] | R_1 [$\Omega \text{ cm}^2$] | Q_1 [$\times 10^{-5}$ S sn cm^{-2}] | n_1 | R_2 [$\times 10^4 \Omega$ cm^2] | Q_2 [$\times 10^{-3}$ S sn cm^{-2}] | n_2 |
|---------------------|---------------------------------|--|---|--------------------|--|---|--------------------|
| $\text{TiN}_{0.92}$ | 14 ± 1 | (0.13 ± 0.02) $\times 10^6$ | $1.59 \pm$ 0.24 | $0.75 \pm$ 0.03 | — | — | — |
| TiN 60°_Inclined | 21 ± 1 | 50 ± 10 | $3.35 \pm$ 0.07 | $0.63 \pm$ 0.04 | $7.35 \pm$ 0.64 | $5.74 \pm$ 0.73 | $0.90 \pm$ 0.01 |
| TiN 60°_ZigZag | 19 ± 3 | 71 ± 8 | $5.27 \pm$ 1.35 | $0.85 \pm$ 0.03 | $2.84 \pm$ 1.25 | $5.26 \pm$ 0.14 | $0.87 \pm$ 0.03 |
| TiN 80°_Inclined | 26 ± 3 | 79 ± 13 | $5.02 \pm$ 1.66 | $0.74 \pm$ 0.02 | $4.31 \pm$ 2.15 | $3.17 \pm$ 0.81 | $0.81 \pm$ 0.04 |
| TiN 80°_ZigZag | 26 ± 6 | 41 ± 3 | $6.73 \pm$ 1.01 | $0.73 \pm$ 0.07 | $0.35 \pm$ 0.16 | $7.115 \pm$ 0.65 | $0.87 \pm$ 0.01 |

It is possible to observe that no significant differences on the corrosion rate (i_{corr}) between $TiN_{0.92}$ thin film with conventional structure and both $TiN_{0.92}$ prepared using $\alpha = 60^\circ$ as deposition angle and also with $TiN_{0.92}$ obtained with an inclination angle of 80° . However, the coating with a deposition angle of 80° and with zigzag-like structure presented a corrosion rate almost 7 times higher than the others $TiN_{0.92}$. It is important to note that the average pore size increased as the deposition angle increased and also from the inclined structure thin film, and thus the corrosion resistance is affected by both thin films' structure and porosity level.

Being Q_1 values related with the passive film formed on the thin film surface, it is possible to observe that as the deposition angle increased the Q_1 values slightly increased from 0° up to 80° , however, when the thin film structure is zigzag-like these values are even higher (figure 48).

Thus, there is a decrease in the quality of the formed passive films.

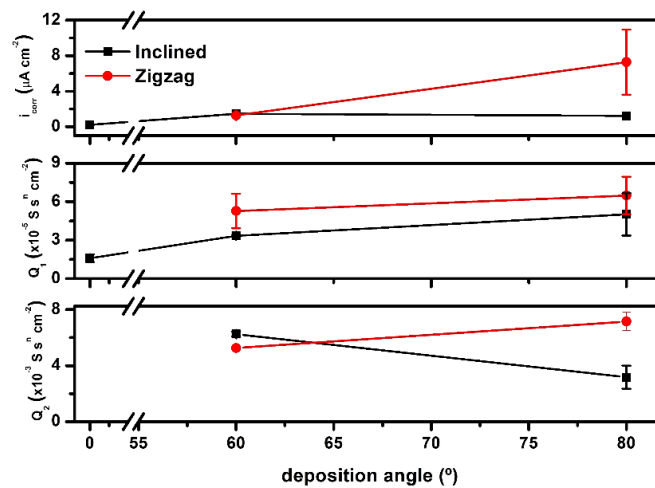


Figure 48 Influence of deposition angle and thin film geometry on corrosion current density (i_{corr}) and Q_1 values of TiN thin films.

Regarding the Q_2 , which is linked to the quality of the passive films formed between (inside) the columns of structure of the $TiN_{0.92}$ thin film, it is possible to observe that when the

deposition angle increased from 60° to 80° , the Q_2 decreased, showing a better quality for $TiN_{0.92}$ films with a deposition angle of 80° .

$TiN_{0.92}$ film obtained with a deposition angle of 80° presented higher average pore size that can facilitate the penetration of the electrolyte, which might lead to a more resistant passive film.

However, $TiN_{0.92}$ having a zigzag-like structure the Q_2 values increased, this complex structure will complicate the electrolyte paths and thus more difficult the formation of the passive film.

Conclusions and personal contribution

This doctoral thesis presents a comprehensive investigation into the influence of nanostructural design on the properties of TiN and (Ti,Al)N coatings deposited by PVD magnetron sputtering technique.

The research focuses on understanding how variations in deposition angle and the creation of inclined and zigzag structures affect the chemical-, structural-, morphological-, thermal-, optical-, electrical-, mechanical-, tribological- and corrosion properties of these coatings.

The study reveals that increasing the deposition angle leads to a decrease in deposition rate and a slight increase in the N/Ti ratio, indicating changes in the growth kinetics and stoichiometry of the coatings. While the coatings maintained a consistent FCC-TiN structure, the microstructure transitioned from dense columnar to porous by changing the inclination angle, significantly impacting surface porosity and pores size. This structural evolution had profound effects on various properties.

In Chapter 3, **Deposition and characterization of TiN and (Ti,Al)N coatings with a normal columnar structure growth**, the findings demonstrate how increasing N₂ flow in TiN coatings and Al content in (Ti,Al)N coatings change the properties.

The findings demonstrate how increased nitrogen flow changed the microstructure and characteristics of TiN by causing it to go from sub-stoichiometric to over-stoichiometric. Denser coatings with V-shaped columnar structures were formed by higher N₂ content, whereas less N₂ content led to less dense structures.

Surface roughness and crystallinity were affected when aluminium was added to the composition of (Ti,Al)N coatings, causing a change from columnar to continuous and homogeneous layers (with a tendency of losing the columnar aspect). The investigation also looked at the coatings' electrical, optical and thermal characteristics. The increase of aluminium concentration in (Ti,Al)N coatings produce smoother surfaces and electrical resistivity reached lower values. In regard to TiN coatings,

increasing the quantity of N_2 often resulted in a decrease in thermal diffusivity and effusivity. Through manipulation of deposition conditions and composition, the research offers useful insights into customizing the characteristics of TiN and (Ti,Al)N coatings for a range of applications. As can be seen from all of the above data, near-stoichiometry coatings are essential for optimal behaviour across the board.

Furthermore, as everything is based on roughness, porosity and nanostructure, composition and morphology are the primary determinants of different attributes.

In Chapter 4, **Deposition and characterization of TiN and (Ti,Al)N coatings with with inclined and zigzag structural designs**, the research studies the influence of different nanostructured designed coatings of TiN and (Ti,Al)N. It is presented the difference between the normal columnar growth, the inclined structure and the zigzag design of the coatings.

While there weren't many expectations going into the study, as it progressed, several unexpected findings emerged. The characteristics of the coatings are significantly influenced by the nanostructure design.

In terms of electrical properties, the surface can change from a conductive one to insulating one as the columns are more inclined, even though the composition is maintained the same.

In thermal characterization, the same behaviour is observed.

The current research evaluated the effects of zigzag and inclined nanostructures on the characteristics of coatings made of TiN and (Ti,Al)N.

The findings showed that higher deposition angle caused the N/Ti ratio to rise and the deposition rate to decrease. The coatings showed some differences in grain size but a similar FCC-TiN structure overall. With increasing inclination angle, SEM research revealed a shift from a dense columnar structure to a more porous one, which had a substantial impact on surface porosity and pore size. Thermal diffusivity and effusivity reduced as a result of this structural development, while reflectivity also fell and colour coordinates changed toward

darker tones. The rougher surfaces' scattering effects led to an increase in electrical resistance.

As the inclination angle rise, the mechanical properties such as adhesion, hardness and elastic modulus similarly reduced because of the weaker columnar bonding and increased porosity. Higher surface porosity and roughness led to an increase in the wear rate and friction coefficient. Porosity and the type of passive layer that developed inside the columnar formations had an impact on corrosion resistance.

To conclude, this research provides valuable insights into the intricate relationship between nanostructural design and the functional properties of TiN and (Ti,Al)N coatings.

These findings demonstrate that tailoring the deposition angle and creating inclined or zigzag structures can significantly modify the thermal, optical, electrical, mechanical, tribological and corrosion properties of these coatings.

This knowledge can be leveraged to engineer coatings with specific properties for various applications, ranging from wear-resistant tools to optical and electronic devices.

The study also underscores the importance of considering the interplay between different properties when designing nanostructured coatings, as optimizing one property may lead to trade-offs in others. Further research in this field can explore the potential of other nanostructural designs and deposition techniques to unlock new possibilities for tailoring the properties of thin film coatings without any change in the composition.

The personal contribution represents the research on the influence of the nanostructural design of TiN and (Ti,Al)N thin films, by varying the deposition angle ($\alpha = 40^\circ, 45^\circ, 60^\circ$ and 80°). Until now, the zigzag structure was studied more in multilayer coatings.

Through this research, it is offered to the industry a way to have huge changes of the properties, buy only changing the

structural design. Therefore, reproducibility is easier and more efficient.

The coatings with adjusted nanostructures are suitable for applications where high porosity is needed, such as medical implants. Moreover, they are useful for purposes which require reduced thermal diffusion as well as higher electrical resistivity.